



UNIVERSITY OF SONORA

DIVISION OF EXACT AND NATURAL SCIENCES
PHYSICS RESEARCH DEPARTMENT

DEVELOPMENT OF THE LUMINOSITY MEASUREMENT SYSTEM FOR THE HIGH LUMINOSITY LARGE HADRON COLLIDER

THESIS

in partial fulfillment of the requirements for the degree of:

Master of Science in Physics

By:

Hedwin Aaron Encinas Acosta

Director:

Dr. José Feliciano Benítez Rubio

Hermosillo, Sonora

August 4, 2021

Universidad de Sonora

Repositorio Institucional UNISON



**"El saber de mis hijos
hará mi grandeza"**



Excepto si se señala otra cosa, la licencia del ítem se describe como openAccess

Acknowledgements

Thanks to my family for their unconditional support and patience and for always being there when I needed them the most, without them I would not be here.

To my friends Carolina, Alejandro and Luisa, for all the help and for making my studies more fun.

To my advisor Dr. José Feliciano Benítez, for always being there to answer my doubts, his patience, and for the opportunity of letting me work in the CMS collaboration.

Finally, thanks to CONACYT for supporting my studies with financial aid.

Abstract

The design and expected performance of the Tracker End-cap Pixel (TEPX) and other subdetectors as luminometers for the CMS experiment at the upcoming High-Luminosity LHC (HL-LHC) is described. The TEPX detector is composed of 4 double sided disks covering a range on $|z|$ from 175 to 265 cm, each one made of 5 rings composed of silicon sensors with a high number of pixels. Disk 4 Ring 1 (TEPXD4R1) will be designated for luminosity measurements only, utilising the same method as the TEPX luminometer, the pixel cluster counting (PCC) method. For the HL-LHC, the goal is to achieve a final uncertainty of 1% for the luminosity measurements. The expected performance and linearity of the TEPX, TEPXD4R1 and other luminometers in terms of statistical precision, for van der Meer (vdM) scan calibration and for physics conditions, are presented. The bandwidth needed for the transfer of the luminosity data and disk needed for storage are estimated.

Resumen

Se describe el diseño y el rendimiento esperado del Tracker End-cap Pixel (TEPX) y otros sub detectores como luminómetros para el experimento CMS, en el próximo LHC de alta luminosidad (HL-LHC). El detector TEPX está compuesto por 4 discos de doble cara que cubren un rango en $|z|$ de 175 a 265 cm, cada uno compuesto por 5 anillos hechos de sensores de silicio con un alto número de píxeles. El Disco 4 Anillo 1 (TEPXD4R1) se designará solo para mediciones de luminosidad, utilizando el mismo método que el luminómetro TEPX, el método de conteo de conjuntos de píxeles (PCC). Para la etapa del HL-LHC, el objetivo es lograr una incertidumbre final de 1% para las mediciones de luminosidad. Se presentan el rendimiento esperado y la linealidad de TEPX, TEPXD4R1 y otros luminómetros en términos de precisión estadística, para la calibración de escaneo de van der Meer (vdM) y para condiciones físicas. El ancho de banda necesario para la transferencia de los datos de luminosidad y el disco necesario para su almacenamiento es estimado.

Table of contents

List of figures	vi
List of tables	vii
1 Introduction	1
1.1 The Standard Model	1
1.2 The Higgs Boson	3
1.3 Particle colliders and detectors	4
1.4 Luminosity	5
2 Experiment Description	7
2.1 The Large Hadron Collider	7
2.2 The CMS detector	9
2.2.1 Silicon tracker	10
2.2.2 CMS calorimetry system	11
2.2.3 Muon Detector	13
2.3 High Luminosity LHC	14
2.4 Tracker End-Cap Pixel luminometer	15
3 Luminometer system description	18
3.1 Pixel Clusters and the PCC method	18
3.2 Cluster coincidence algorithm	19
3.3 Calibration using the van der Meer method	20
3.4 Data acquisition	22
3.4.1 Other luminometers	24
3.4.2 Data transfer rates for all luminometers	28
4 Analysis and Results	30
4.1 Linearity of the TEPX luminometers	30
4.2 Statistical precision for Physics data taking	33
4.3 Statistical precision for vdM	34
4.3.1 Toy simulation of the vdM scan	34
4.4 Comparison to other luminometers	37
5 Conclusion and Summary	39
References	40

List of figures

1.1	Standard model of particles	3
2.1	CERN accelerator complex.	8
2.2	CMS detector diagram	9
2.3	CMS tracker.	10
2.4	Hadron forward wedge.	12
2.5	One quarter of the CMS muon system.	13
2.6	schedule of the LHC.	15
2.7	Diagram of the Phase-2 inner tracker upgrade.	16
3.1	Pixel cluster selection algorithm	18
3.2	Regions where two-fold coincidences can occur in r and ϕ	20
3.3	vdM scan process.	21
3.4	Histogram of the mean number of pixel clusters per bunch crossing (BX) measured by the Phase-1 pixel detector.	22
3.5	Different subsystems and luminometers at CMS.	25
3.6	Outer tracker layout.	25
3.7	Example of an OT layer 6 ladder and the stub selection process.	26
3.8	Simulated expected number of stubs per ladder per event.	27
3.9	Expected rates of trigger primitives per DT chamber	28
4.1	Linearity of TEPX for pixel clusters.	31
4.2	Linearity of TEPXD4R1 for pixel clusters.	31
4.3	Linearity of TEPX for two-fold coincidences.	32
4.4	Linearity of TEPXD4R1 for two-fold coincidences.	32
4.5	Simulated rate measurements of the vdM toy study for TEPX.	35
4.6	Simulated rate measurements of the vdM toy study for TEPXD4R1.	35

List of tables

1.1	Fundamental forces and the fermions	2
2.1	Radius and number of pixel modules that comprise the rings of the TEPX subdetector.	17
3.1	Memory bits required per histogram bin for the TEPX luminometers.	24
3.2	Data transfer rates for the TEPX luminometers.	24
3.3	Memory bits required per histogram bin for all luminometers.	29
3.4	Data transfer rates for the different luminometers.	29
4.1	Statistical precision of the TEPX luminometers in % for pileup 200.	33
4.2	Statistical precision of the TEPX luminometers in % for pileup 0.5.	34
4.3	Results from the vdM toy study for 1 bx and 150 bx.	37
4.4	Statistical precision in % for pileup 200 for the different luminometers.	37
4.5	Statistical precision in % for pileup 0.5 for the different luminometers.	38
4.6	Results from the vdM toy study for 1 bx and 150 bx for the different luminometers.	38

Chapter 1

Introduction

The Standard Model (SM) in particle physics is the theory that describes the interactions between three fundamental forces, out of the four known (gravitational, electromagnetic, strong and weak), and the known fundamental particles. The gravitational force is not included in the SM, since the magnitude of its strength is neglectable in comparison with the other three forces.

The theory was developed throughout the second half of the 20th century by the hard work of physicists around the world, with the current formulation being established in the mid 70s.

In high energy physics, precise measurements are the core of any experiment. A key quantity is the luminosity, and its precise determination is an important aspect. The search for low incidence processes whose observation is not yet confirmed, such as the $H \rightarrow \gamma + Z$ channel, relies in the accumulation and precise measurements of luminosity.

1.1 The Standard Model

The SM classifies all known fundamental particles into two major groups, fermions, particles with spin $1/2$, and bosons, particles responsible for mediating the fundamental forces and integer spin. Fermions are divided into two families of particles, leptons and quarks. There exist 6 leptons in the SM, first there are charged particles, electrons (e), muons (μ) and the taus (τ) with an electric charge of -1 and spin of $1/2$. To each of these particles corresponds a chargeless neutrino, ν_e, ν_μ and ν_τ .

Leptons can be found in nature existing by themselves, and along with quarks, comprise the majority of matter in the universe. Electrons can be found “circling” atoms, muons can be found raining from the sky due to cosmic rays interacting with particles on the

atmosphere and, while taus are a little bit tricky to find due to their short life time (2.9×10^{-13} s), they do exist by themselves; however, this cannot be said for quarks, since they are only found forming other particles called hadrons. Hadrons can be a combination of two quarks called mesons, usually a quark-antiquark combination or a combination of three quarks called baryons, an example of a meson would be a pion (π). Neutrons and protons are made by a combination of three quarks, so they are classified as baryons. Quarks were first theorised by Murray Gell-Mann and George Zweig in 1964 and later discovered by experiments conducted at the Stanford Linear Accelerator Center (SLAC) in 1968 [1]. A total of 6 quarks were discovered over a period of 26 years, in order of discovery these are: up (u) (1968), down (d) (1968), strange (s) (1968), charm (c) (1974), bottom (b) (1977), top (t) (1995).

Quarks are the only fermions that interact with all three fundamental forces included in the SM, they possess electric charge, color charge (the strong force equivalent of electric charge), weak charge, mass and spin $1/2$ as do all fermions. The u , c and t quarks have an electric charge of $2/3$ and the d , s and b quark have an electric charge of $-1/3$. Table 1.1 shows which fermions interact with the different forces.

Table 1.1 Fundamental forces and the fermions they interact with [2].

		Electromagnetic	Strong	Weak
Quarks	u c t	✓	✓	✓
	d s b			
Fermions	e μ τ	✓		✓
	ν_e ν_μ ν_τ			✓

For each fermion that exists, there corresponds an antiparticle. Antiparticles have the same properties as their counterparts, with the only distinction being that they possess opposite electric charge. If an antiparticle comes in contact with a particle, let's say a positron (anti-electron) and an electron, they would annihilate each other.

The SM also comprises particles with integer spin such as the bosons. Bosons are force carrier particles in charge of mediating the interactions between particles, let's take classical electromagnetism as an example. Classically, the electrostatic force is described by a scalar field and while this is sufficient for classical electromagnetism, it is fundamentally wrong for quantum dynamics. This would mean that two charged particles interact with each other at a distance, without contact of any kind [2].

In particle physics, each fundamental force is described by a quantum field theory (QFT) and the interaction between two particles are mediated by gauge boson, a spin-1 particle. For example, the electromagnetic force is described by Quantum Electrodynamics (QED) and mediated by the photon, a particle with no charge or mass. The strong force is described by Quantum Chromodynamics (QCD) and mediated by a gluon, which has no mass or electric charge, gluons are what bind quarks together to form hadron and like quarks, are only found in these bind states. Finally the weak force is mediated by the Z and W^\pm bosons, massive particles with 0 and ± 1 electric charge respectively [2]. The Higgs boson is the last member of the SM, unlike the gauge bosons, the Higgs has spin-0 and is the only fundamental scalar discovered. Figure 1.1 shows all the particles included in the SM.

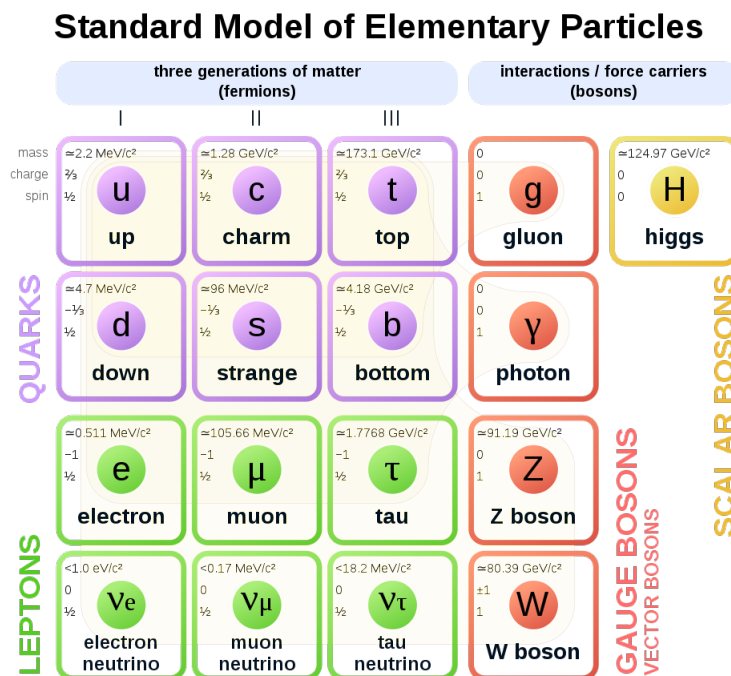


Fig. 1.1 Particles that compose the standard model and their properties [3].

1.2 The Higgs Boson

The Higgs boson is the latest member of the SM, first theorised in 1964 by Peter Higgs, Robert Brout, François Englert, Gerald Guralnik, C. Richard Hagen and Tom Kibble and later discovered by the ATLAS and CMS experiments at the Large Hadron Collider (LHC) in Geneva Switzerland in 2012. The experiment consisted in proton-proton collisions with

a center of mass energy of 7 and 8 TeV, the data analysed from the experiment corresponds to five decay channels: $\gamma\gamma$, ZZ , W^+W^- , $\tau^+\tau^-$ and $b\bar{b}$. With the discovery being made in the $\gamma\gamma$ and ZZ channels [4][5]. The Higgs plays a vital role in the SM, it is responsible for the mechanism that gives every particle their mass. It has a mass of 125.78 ± 0.26 GeV [6], consistent with SM predictions, it does not possess electric or color charge and it is the only fundamental scalar and spin-0 boson.

The discovery of the Higgs is one of the greatest accomplishments of the SM, it shows the hard work that has gone in to developing the theories that compose it [2].

1.3 Particle colliders and detectors

The discovery of the Higgs marked an important milestone in particle physics, however, this feat required the construction of the LHC, the largest and most powerful particle collider in the world. Particle colliders are the devices where particle physics experiments are conducted. As their name suggests, colliders propel bunches of particles like electrons, protons, positrons, etc. using powerful electromagnetic/electrostatic fields, and make them collide with a fixed target or other particles. These collisions produce other particles that are measured by particle detectors in the site of the collision, this is the means by which new particles are discovered.

Particle colliders come in two types: linear and circular. Linear colliders use changing electromagnetic fields to accelerate particles along a straight beam path and make them collide with a fixed target, where particle detectors are located, an example of the linear accelerator would be the Stanford Linear Accelerator Center. While circular colliders to accelerate bunches of particles in opposite directions in a circular beam fashion, making them collide at key points around the accelerator where particle detectors are located. The LHC is an example of a circular collider.

The majority of modern experiments in particle physics are conducted in circular colliders, since these are the only ones that can provide the center of mass energy needed to produce heavier particles, like the Higgs or the Top quark. Due to the high energy requirements, circular accelerators are very complex machines composed of many parts, but for the sake of this work, we will only focus on the particle detectors. Modern particle detectors are composed of many layers of subdetectors tasked with measuring the effects that particles have on them, when they pass through. For example, a subdetector may measure the number of hits, tracks or pixel clusters activated during a collision.

The layout of the detector will change to best accommodate the experiments being performed, but in general, these subdetectors can be classified into three categories: Tracking devices, to track the path of a particle; calorimeters, they measure the energy

deposited by a particle when it hits and particle identifiers, that use various techniques and the measurements from other subdetectors, to identify the different particles produced in a collision [7]. The CMS detector and the LHC is an example of a layered particle detector.

Finally, two parameters are used to measure the efficiency of a particle collider, the beam energy and the luminosity. The higher the beam energy, the more particles can be created and thus the higher chance that new effects can be observed. The luminosity (\mathcal{L}) is a measure of the efficiency of a particle collider to produce meaningful interaction between colliding bunches of particles.

1.4 Luminosity

As mentioned before, the LHC collides particles by grouping them into bunches, where trains of N_b bunches are made. The groups of bunches are circulated both clockwise and anticlockwise and are forced to cross at specific detection points, where several interactions occur. A collision between bunches is called an event, and several particle interactions are produced during these events, the quantity that measures the ability of any particle collider to produce these useful interactions is called Luminosity. Thus, the event rate R , of a particular type p , with cross-section σ_p , is given by [8]:

$$R = \mathcal{L}_{ins} \sigma_p \quad (1.1)$$

Where the instantaneous luminosity, \mathcal{L}_{ins} , is the proportionality constant, the cross section is the likelihood of that event taking place and has units of cm^2 , thus the luminosity has units of $cm^{-2}s^{-1}$ [8]. Since the probability of a rare event increases the more the rate of interactions grows, the luminosity is a key figure in the performance of a particle collider.

Let's consider N_b colliding bunches, assuming all the bunches have a head-on collision, the luminosity of all the colliding bunches is given by [9]:

$$\mathcal{L}_{ins} = N_b N_1 N_2 f \int_{-\infty}^{\infty} dx \int_{-\infty}^{\infty} dy \rho_1(x, y) \rho_2(x, y) \quad (1.2)$$

where $N_{1,2}$ are the particles per bunch, f is the revolution frequency and $\rho_{1,2}$ are the normalized densities in the transverse plane. Assuming that the normalized densities are uncorrelated in all planes, the distribution functions can be factorized as:

$$\rho_i(x, y) = \rho(x) \rho(y) \text{ where } i=1,2 \quad (1.3)$$

Thus, equation 1.2 can be writhe as

$$\mathcal{L}_{ins} = N_b N_1 N_2 f \int_{-\infty}^{\infty} \rho_1(x) \rho_2(x) dx \int_{-\infty}^{\infty} dy \rho_1(y) \rho_2(y) \quad (1.4)$$

For the case of head-on colliding bunches, a Gaussian charge distribution can be used, equation 1.3 can be written

$$\rho(u) = \frac{1}{\sqrt{2\pi}\sigma_u} \exp\left(-\frac{u^2}{2\sigma_u^2}\right) \text{ where } u=x,y. \quad (1.5)$$

using this, equation 1.4 can be integrated analytically, giving

$$\mathcal{L}_{ins} = \frac{N_1 N_2 N_b f}{2\pi \sqrt{\sigma_{x1}^2 + \sigma_{x2}^2} \sqrt{\sigma_{y1}^2 + \sigma_{y2}^2}} \quad (1.6)$$

In practice, the bunch densities in the transverse plane are not known and a calibration of the detectors has to be done, in order to obtain these values. At the LHC, this is done by a dedicated machine setup. The performances of a particle collider over a period of time is given by the integrated luminosity :

$$L = \int \mathcal{L}_{ins}(t) dt \quad (1.7)$$

The average number of interaction per bunch crossing is given by the pileup, μ , and directly proportional to the luminosity

$$\mu = \frac{\mathcal{L}_{ins} \sigma_{tot}}{f} \quad (1.8)$$

where the σ_{tot} is the total cross-section of the collided particles [9].

It is worth noting that a head-on collision is not always the case. The bunches can collide in different ways, such as an off-set a crossing angle or both. In these cases, the overlapping integral in equation 1.2 is reduced. This is done by applying a reduction factor to equation 1.4 [9], however, this work is only concerned with the head-on collision case, the other scenarios can be found in [8].

Chapter 2

Experiment Description

2.1 The Large Hadron Collider

The LHC is one of the most powerful particle collider in the world, it started construction in 1998 on the France–Switzerland border near Geneva, using the 26.7 km tunnel, constructed for the CERN LEP machine. It came into operation on the 10 of September of 2008, and it is the latest addition to the CERN accelerator complex. It was first approved on December 1994 by the CERN council, with a center-of-mass-energy of 14 Tev [10].

The LHC consists of two separate rings, kept in an ultrahigh vacuum, where two the beams of particles are located. To achieve the circular motion of the beams, 1232 dipole magnets are used to maintain trajectory, and 392 quadrupole magnets are used to keep the beams focused. Near the interaction points, stronger quadruple magnets are used to increase the probability of interaction between the beams. These magnets are made of coils of special superconductive cable, cooled to a temperature of 1.8 K with superfluid helium, producing an electromagnetic field of above 8 T [10].

The beams in each ring are made of bunches for particles traveling near the speed of light. These bunches can be made of protons or ions (like lead nucleons), depending on the running experiment, however, the majority of events at the LHC are produced by proton-proton (pp) bunch collision.

A diagram of CERN's accelerator complex can be seen in Figure 2.1. The proton bunches start as ionised hydrogen gas and are accelerated to an energy of 50 MeV, by the Linac 2 linear accelerator. Once they leave the Linac 2, they are further accelerated to an energy of 1.4 GeV by the Proton Synchrotron Booster (PSB) and dumped on the Proton Synchrotron (PS). In the PS, the bunches are accelerated to an energy of 25 GeV and arranged into a bunch trains, with a spacing of 25 ns, in total, one orbit contains 3564 bunches, arranged in to several trains. Finally, the bunches pass from the PS to the Super Proton Synchrotron

(SPS), where they are injected into the LHC with an energy of 450 GeV. In the LHC, the beams reach a peak energy of 6.5 TeV, and are made to collide in one of the 4 detectors, ALICE, ATLAS, CMS and the LHCb.

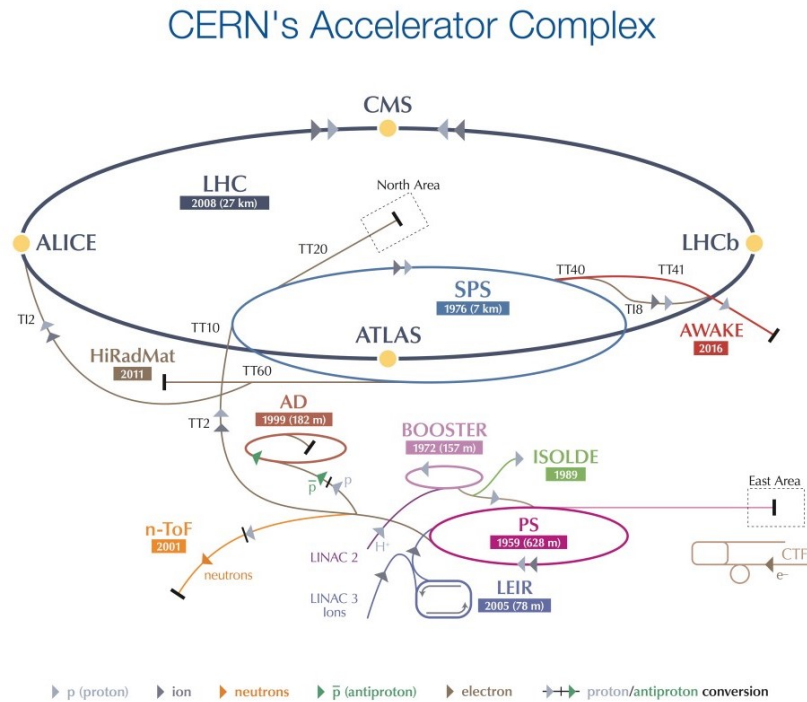


Fig. 2.1 A diagram of the CERN accelerator complex [11].

The four detectors are tasked with measuring all the particles produced in pp collisions. Two specialized detectors are integrated to the LHC, ALICE and LHCb. ALICE is dedicated to heavy ion collisions physics, where the quark-gluon plasma is studied. The LHCb investigated the differences between matter and antimatter, by studying the “beauty quark” [12].

The two remaining detectors, CMS and ATLAS, are general purpose detectors, tasked with studying a wide range of physics, from the search of the Higgs boson, to extra dimensions and particles that could make the dark matter in the universe [13].

Two operation runs have been completed so far at the LHC, and two long shutdowns, where maintenance and several minor upgrades were made to the machine. Run 1 lasted from 2010-2012, while Run 2 lasted from 2015-2018. As of Run 2, the LHC has achieved a peak luminosity of $2 \times 10^{-34} \text{ cm}^{-2} \text{ s}^{-1}$, two times the amount for which the LHC was designed. The integrated luminosity, since the LHC began operations, has reached 160 fb^{-1} for the ATLAS and CMS experiments [14].

2.2 The CMS detector

The Compact Muon Solenoid (CMS) experiment is one of the four major experiments currently running in the LHC, and along with ATLAS, one of the two high luminosity experiments at CERN. It receives its name from the huge solenoid magnet, from which the detector is built around. This solenoid takes the form of a coil made of super conductive wire, capable of producing an electromagnetic field of 4 T. The field is confined by a steel yoke, that weights 14,000 tones.

CMS is a layered detector, 21 m in length, with a height and width of 15 m, and it is composed of four main subdetectors, the inner silicon tracker, electromagnetic and hadron calorimeters and the muon detectors. The strong magnetic field produced by the detector's solenoid, separates the particles produced in the coalitions and provides a better momentum resolution. Figure 2.2 shows a diagram of the detectors layout.

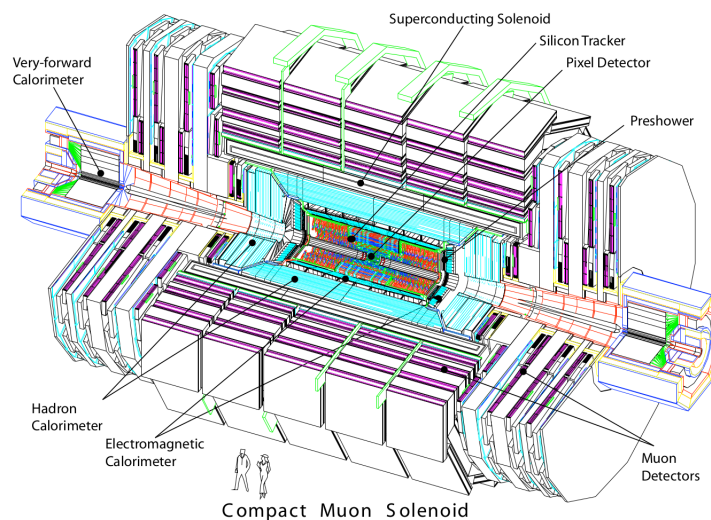


Fig. 2.2 Diagram of the CMS detector showing the various subdetectors that comprise it [15].

The CMS experiment has a broad range of goals in particle physics, from studying the SM in search of new particles and phenomena, to searching for extra dimensions and discovering new particles that could make the dark matter in the universe. The experiment has achieved great things in the scientific community, however, one of its greatest, was the discovery of the Higgs boson alongside the ATLAS experiment in 2012. In the next subsection a brief description of the different subdetectors is provided [15].

2.2.1 Silicon tracker

At the heart of the CMS detector lies the inner silicon tracker. As its name suggests, the purpose of this subdetector is to reconstruct the track of charged particles generated during collisions, by using silicon strips and pixels to register the paths of charged particles. Once the track of a charged particle is reconstructed, its momentum can be extracted, by calculating the curb of its trajectory, produced by the electromagnetic field. Also, the vertex, the origin of the track, can be determined. The Tracker, which consists of an Inner Tracker (pixels) and an Outer Tracker (strips), is the first subdetector encountered by the particles, and thus the smallest, with an outer radius of 110 cm and a total length of 5.4 m, Figure 2.3 shows the layout of the inner tracker.

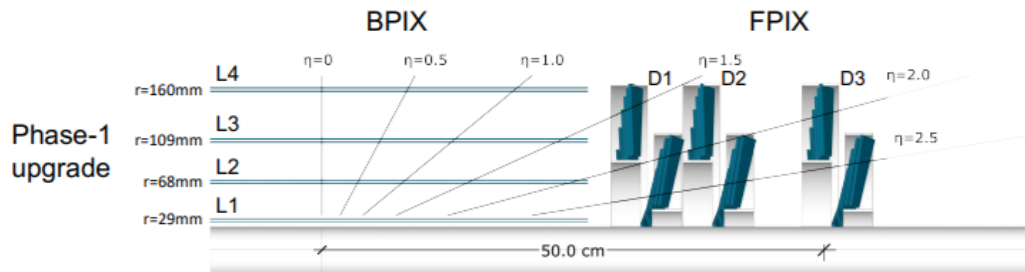


Fig. 2.3 Diagram showing the layout of the CMS Phase-1 inner tracker. The barrel pixel detector (BPIX) and the forward disks pixel detector (FPIX) are shown [16].

The tracker is divided into two subtrackers: one is the silicon strip tracker, made of 9.6 million silicon strips. This subtracker is divided in two parts: the Tracker Inner Barrel (TIB) and the Tracker Outer Barrel (TOB). The TIB is made of 4 layers that cover up to $|z| < 65$ cm. The TOB has 6 layers, and a coverage of $|z| < 110$ cm. The encaps are again divided into two regions, Tracker End Cap (TEC) and Tracker Inner Disk (TID). The TEC is composed of 9 disks that extend in the region $120 \text{ cm} < |z| < 280$ cm, while the TID has 3 disks that fill the gaps in between the TIB and the TEC. The TEC and the TID are made of rings centered on the beam, and possess stripst that point towards the beam. The strip tracker encompass and area of 200 m^2 , and it is made of almost 15,400 modules, running at a temperature of -20°C .

The other subtracker is the pixel tracker, made of three layers of barrels possessing a radius of 4.4 cm, 7.3 cm and 10.2 cm with a length of 53 cm, and consisting of 66 million pixels. In each end of the barrels, two end cap disks reside, extending from 6 to 15 cm in radius and located at $|z| = 34.5$ cm and 44.5 cm, in total, the pixel tracker has an area of roughly 1m^2

768 pixel modules are housed in the barrel, all arranged into half lathers of 4 identical

modules. The end cap disks are designed in a turbine-like geometry, with blades rotated 20° . The blades are made of 7 different pixel modules, with a total of 768 modules being housed in the end cap disks [15].

2.2.2 CMS calorimetry system

The calorimetry system of the CMS detector is composed of two types of calorimeters: the electromagnetic and hadronic calorimeters. Both subdetectors form a complete and hermetic calorimetry system with a coverage of $-5 < \eta < 5$. The calorimeters are a crucial part of the CMS detector, since the identification and reconstruction of photons and electrons is done using measurements from the calorimetry system, as well as the measurements of jets and missing transverse momentum. A brief description of the electromagnetic and hadronic calorimeter is provided below.

Electromagnetic calorimeter

The electromagnetic calorimeter (ECAL) measures the energy of electrons and photons. Once charged particles enter the ECAL, they produce a shower of secondary electrons and photons. These electrons pass through the lead tungstate ($PbWO_4$) crystals, which scintillates when electrons hit their crystalline structure, producing light that is measured by photodiodes in the calorimeter.

It is made of 75848 tungstate crystals [17]. It is an hermetic, homogeneous calorimeter composed of a central barrel and two end-caps. Silicon avalanche photodiodes (APDs) are used in the barrel and vacuum phototriodes (VPTs) in the end caps.

The central barrel has an inner radius of 129 cm and a structure of 36 “supermodules”, that cover half the barrel’s length. It has a coverage of $|\eta| < 1.479$. The APDs used on the barrel have an active area of $5 \times 5 \text{ mm}^2$, and two of them are glued to the back of each crystal.

The two end caps have a pseudorapidity range of $1.479 < |\eta| < 3$, and are located at a distance of 314 cm from the vertex. It consists of crystals with an identical shape, grouped in mechanical units of 5×5 [15].

Hadron calorimeter

The Hadron calorimeter (HCAL), along with the ECAL, form a complete and hermetic calorimetry system with the purpose of measuring jets and missing transverse energy. The HCAL surrounds the ECAL and its design is heavily influenced by the magnet parameters, since it is located inside the solenoid magnet. The HCAL is divided into 4 parts: the hadron

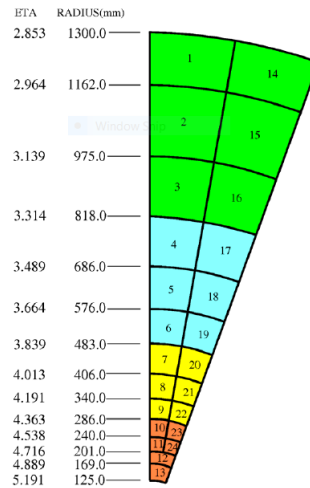


Fig. 2.4 And $r-\phi$ view of a HF wedge.

barrel (HB), hadron outer (HO), hadron endcap (HE) and hadron forward. The absorber material is brass since it has a short interaction length, is non-magnetic and is easy to machine. Tile/fiber technology, embedded between the absorber plates, is used to detect the particle showers. The technology consists of plastic scintillator tiles embedded with wavelength-shifting (WLS) fibers. The fibers are connected to high-attenuation-length clear fibers that carry the light to the readout system.

The photodetection readout is handled by multi-channel hybrid photodiodes (HPDs).

The HB has an inner radius of 1777 mm and an outer radius of 2876.5 mm and has 17 scintillator layers and is composed of 2 half barrels covering a range of $-1.4 < \eta < 1.4$, resulting in a total of 2304 towers. The HO covers a region of $-1.26 < \eta < 1.26$ and it contains scintillators with a thickness of 10 mm, lining the outside of the outer vacuum tank of the solenoid. The HE consists of 14 towers with a range of $1.3 < \eta < 3.0$. It is made entirely of brass plates, with a thickness of 78 mm.

The HF calorimeter has a range of $3 < \eta < 5$ and is made of steel and quartz fibers. It is located 11.2 m from the interaction point, providing fast collection of Cherenkov light. The modules of the HF are constructed of 18 wedges arranged in a non-projective geometry, Figure 2.4 shows and $r-\phi$ view of an HF wedge. The quartz fibers have a diameter of 0.6 mm and are placed 5 mm apart, forming a square grid. Two different lengths are used for the quartz fibers, 1.43 m and 1.65, effectively creating 2 longitudinal samplings. In total, 13 towers exist in η with a size of $\Delta\eta \approx 0.175$, except for the lowest and highest- η towers, which have a size of $\Delta\eta \approx 0.1$ and $\Delta\eta \approx 0.3$ respectively. A $\Delta\phi \approx 10^\circ$ exists for all towers but the highest- η tower, which has a segmentation of $\Delta\phi \approx 20^\circ$. In total the HF calorimeter consist of 900 towers and 1800 channels [15].

2.2.3 Muon Detector

The last subdetector of the CMS experiment is the muon detector system located in the magnet return yokes. The muon system consists of 3 types of gaseous detectors, used to detect muons and their momenta. These detectors are: the drift tube chambers (DT), the cathode strips chambers (CSC) and the resistive plate chamber (RPC). These detector are distributed across the 2 central parts of the muon detector, the barrel and endcap sessions, with a coverage of $|\eta| < 1.2$ and $|\eta| < 2.4$ respectively. The distribution of these detectors is shown in Figure 2.5.

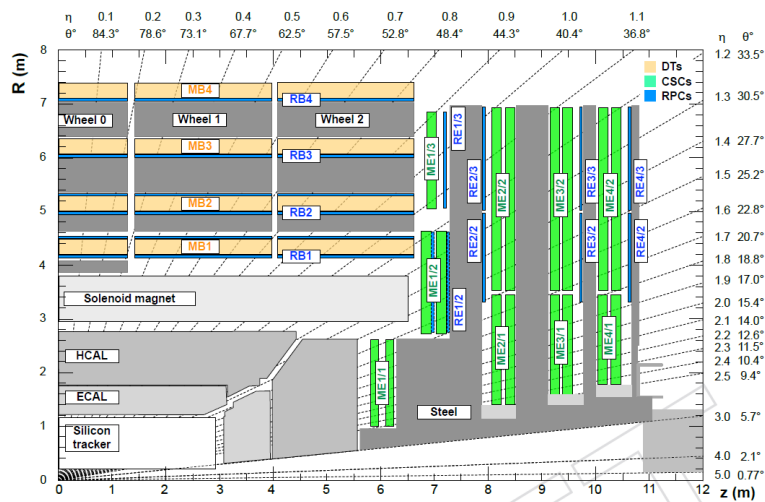


Fig. 2.5 The diagram shows the layout of one quarter of the muon system at CMS [15].

The barrel DT detector has a coverage of $|\eta| < 1.2$, and consist of 250 chambers arranged in 4 layers inside the magnet return yoke, at a radii of approximately 4, 4.9, 5.9 and 7 meters from the beam line. The basic element of the DT detectors are cells, with a transverse size of $42 \times 13 \text{ mm}^2$, filled with a gas mixture of 85% Ar and 15% CO_2 [18]. The cells have a gold-plated stainless steel anode wire, connected at their center. The wire has a diameter of $50 \mu\text{m}$ and it operates at a voltage of +3600 V. The barrel detectors are divided into 12 sectors, each covering 30° in the azimuthal direction.

Installed on the encap regions, the CSC chambers are installed, covering a range of $0.9 < \eta < 2.4$. Their fast response time and their tolerance to non-uniform magnetic fields, makes the perfect for the high muon rates and background levels found in this region. The 6 layers of the CSC measure the muon positions in 2 coordinates. The cathode strips provide precise measurements on the $r-\phi$ bending plane, while the wires provide a coarse measurement in the radial direction. Each layer of the CSC contains 80 cathode strips with anode wires, of diameter $50 \mu\text{m}$, running almost parallel to the cathodes.

In total, the 2 encaps are comprised of 468 CSC chambers, filled with a gas mixture of 50% CO_2 , 40% Ar and 10% CF_4 [18].

The RPC detectors is located in the barrel and encap regions of the muons system, complementing the DT and CSC detectors. It covers a region of $|\eta| < 1.6$ and it provides fast, independent trigger events. The RPC are double-gap chambers, each gap consisting of 2 mm thick resistive bakelite plates, separated by a 2 mm thick gas gap. Readout strips are aligned in the η direction in between the gas gaps. The gaps are filled with a gas mixture of 95.2% Freon ($C_2H_2F_4$), 4.5% isobutane ($i-C_4H_{10}$), and 0.3% sulphur hexafluoride (SF_6). Water vapor is added to reach a mixture humidity of 40%-50% [18].

2.3 High Luminosity LHC

The LHC is the most powerful particle collider in the world, and it is to remain the most powerful for the next two decades. To ensure this, the LHC will receive major upgrades during the 2020s, to increase its luminosity by a factor of 5 beyond the original design. About 10 years will be needed to study and prototype the technologies required for the new High Luminosity LHC (HL-LHC). The HL-LHC project was created at the end of 2010 by CERN, as a response to the European strategy for particle physics, to fully exploit the capabilities of the LHC. The project was approved on 30 of May of 2013 by the CERN council in charge at the time. For the next decade the HL-LHC is the major construction project of CERN. Several new technologies will be used to achieve the luminosity goal, some of them include: superconducting magnets capable of producing a magnetic field of 11 to 12 T, superconducting cavities, compact and with phase control, for beam rotation, long high-power superconducting links with zero energy dissipation and new technologies for beam collimation [19].



Fig. 2.6 The past and future schedule of the LHC. The red line corresponds to the center-of-mass-energy of the pp collisions, while the light-red line shows the expected luminosity [20].

Figure 2.6 shows the schedule of the LHC up until 2025, where the new phase of the LHC, the HL-LHC, will begin. After reaching a center-of-mass-energy of 13 during 2015, the LHC has doubled the luminosity for which it was designed, as of the end of Run 2.

The main objectives of the HL-LHC is to reach a peak luminosity of $5 \text{ to } 7.5 \times 10^{34} \text{ cm}^{-2}\text{s}^{-1}$, and an integrated luminosity of 250 fb^{-1} per year, with the goal of reaching a total integrated luminosity of 3000 fb^{-1} , in the first 12 years of the machines operation. For this, intensive studies have, and are, being conducted to determine the hardware and the configuration needed to achieve these goals.

The new hardware of the HL-LHC is to be installed during the third long shutdown (LS3). To ensure that the integrated luminosity goal is met, all equipment is being designed with a 50% margin in regards to the required luminosity. This means that the High Luminosity LHC can reach peak luminosity valued of $7 \text{ to } 7.5 \times 10^{34} \text{ cm}^{-2}\text{s}^{-1}$, this will mean an increase in total pileup (rate of pp collision per bunch crossing) up to 200 [19].

2.4 Tracker End-Cap Pixel luminometer

Along with the new HL-LHC upgrade, several upgrades will come to the CMS detector to accommodate the new luminosity and pileup requirements. The tracker, muon end caps,

trigger and beam radiation protection are just a few of the new upgrades scheduled for the CMS detector. However, the focus of this work will be solely on the tracker upgrades, more specifically, the inner tracker end cap pixel (TEPX) luminometer.

For Phase-2 of the CMS tracking the entire existing pixel and strip tracker will be replaced. Figure 2.7 shows the r-z layout of the three sections of the Phase-2 inner tracker: the tracker barrel pixel (TBPX), composed of four cylindrical layers of modules, the tracker's forward (TFPX) and the tracker end-cap (TEPX) pixel detectors, made of 8 and 4 disks of pixel modules respectively. The new tracker will include: increased granularity, forward acceptance and radiation hardness as well as compatibility with longer trigger latency and higher data rates. The silicon pixel modules will have a thickness of 100-150 μm , while the pixel cells will have an area of $2500 \mu\text{m}^2$ ($25 \times 100 \mu\text{m}^2$) [21][22]. Two types of modules will be used in the inner tracker, modules with 2 and 4 pixel chips. The modules will be arranged in 2×1 and 2×2 , these modules are depicted as green and yellow respectively in Figure 2.7. TBPX and TFPX will be composed of both types of modules, while TEPX will only use 2×2 modules [22].

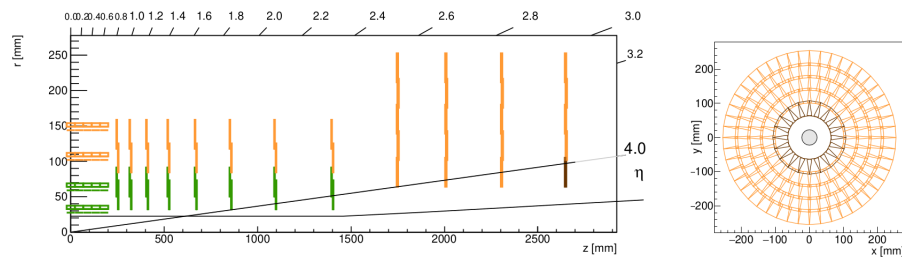


Fig. 2.7 *Lefts*: Diagram of the Phase-2 inner tracker upgrade. The last four yellow lines between 1700 mm and 2700 mm, correspond to the TEPX subdetector. *Right*: Front view of one of the disks of the TEPX subdetector [22].

For Phase-2 the TEPX portion of the tracker will be designated for tracking and luminosity measurements, while disk 4 ring 1 (TEPXD4R1) of the detector will be designated for luminosity measurements only. The TEPX detector is located at each extremity of the tracker of the CMS detector, with a range from 175 cm to 265 cm on the $|z|$ direction and a radius between 63 mm and 255 mm. The detector is composed of 4 double sided disks, each one made of 5 concentric rings of pixel modules. To guarantee hermetic coverage, each ring has a different number of pixel modules. TEPX is composed of 800 million pixels, distributed over an area of 2m^2 , and will operate at trigger frequency of 75KHz during physics runs. Table 2.1 shows the number of modules per ring, as well as the radius of each ring.

Table 2.1 Table shows the inner (r_{in}) and outer (r_{out}) radius, as well as the number of pixel modules that comprise each ring of each disk of the TEPX subdetector

Ring	1	2	3	4	5
r_{in} (mm)	62.9	100.55	137.85	174.45	210.5
r_{out} (mm)	107.69	144.99	182.09	218.56	254.51
No. of modules	20	28	36	44	48

The innermost ring of the last disk, disk 4 ring 1 (TEPXD4R1), lies beyond a pseudorapidity of $|\eta| = 4$ and due to the low number of tracking points in this region, this ring will be designated for luminosity measurements only. The ring consists of 20 modules, and it has an inner radius of 62.9 mm and an outer radius of 107.69 mm. Finally, the luminometer may run at a trigger frequency of 825kHz to several MHz.

Luminosity measurements with the TEPX's detectors will be carried out using the Pixel cluster counting (PCC) method described in the next chapter.

Chapter 3

Luminometer system description

3.1 Pixel Clusters and the PCC method

Luminosity measurements at CMS are provided by the several luminometers in the detector. Each luminometer measures the event rate by reading out a specific quantity of objects observed by the detector, These can be for example clusters, coincidences or tracks. For the TEPX luminometers these objects are pixel clusters and coincidences, using the pixel cluster counting (PCC) method to provide offline luminosity measurements. This method was one of the main source of luminosity measurements for CMS, during the 2016-2018 data taking period, and it is expected to be the same for the Phase-2 upgrade.

The clustering algorithm is very complex, but striping it down to the most simple example: the algorithm considers a cluster of pixels only if two hits, or more, activate neighboring pixels horizontally, vertically or diagonally, within the same module. Figure3.1 shows an example of this.

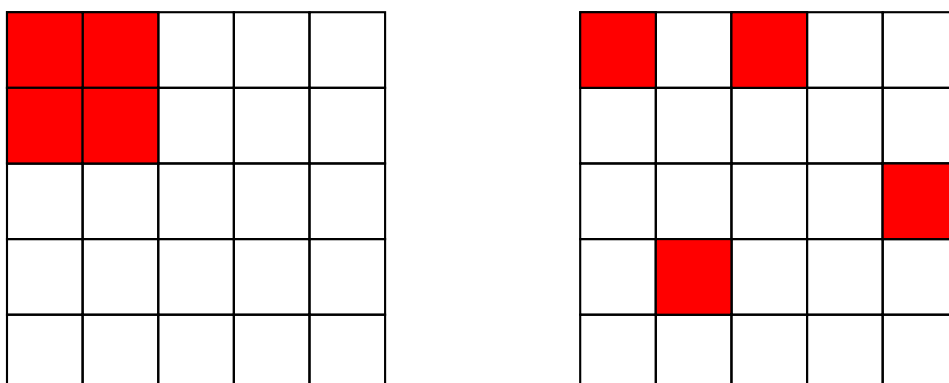


Fig. 3.1 The figure shows a representation of the pixel modules, *left*: four hits (red) on four neighbouring pixels, these is considered a pixel cluster by the clustering algorithm. *right*: the hits activate random pixel in the module, these will not be considered as a cluster by the clustering algorithm.

A hit occurs when a charged particle passes through a silicon pixel, depositing an amount of energy in the pixel. The PCC method takes advantage of the high densities of pixels, and the relative low occupancy of the CMS tracker, to provide precise luminosity measurements, with good stable measurements over time. The number of pixel clusters activated, per bunch crossing, is a linear function of the number of proton-proton interactions per bunch crossing (pileup). During several zero-bias events, where the only requirement is that the bunches pass through one another on the interaction point, a mean number of pixel clusters, $\langle N_{\text{cluster}} \rangle$, is activated:

$$\langle N_{\text{cluster}} \rangle \equiv \langle N_{\text{cluster/int}} \rangle \mu \quad (3.1)$$

where $\langle N_{\text{cluster/int}} \rangle$ is the mean number of clusters activated per interaction and μ is the pileup. Using equation 1.8 and 3.1, a calibration constant between the mean number of pixel cluster and the instantaneous luminosity can be defined:

$$\langle N_{\text{cluster}} \rangle \equiv \frac{\sigma_{\text{vis}}}{f} \mathcal{L}_{\text{ins}} \quad (3.2)$$

where the calibration constant, σ_{vis} , is

$$\sigma_{\text{vis}} = \sigma_{\text{tot}} \langle N_{\text{cluster/int}} \rangle \quad (3.3)$$

The value of σ_{vis} is determined using a van der Meer (vdM) scan, with

$$\sigma_{\text{vis}} = \frac{\langle N_{\text{cluster/vdM}} \rangle f}{\mathcal{L}_{\text{ins/vdM}}} \quad (3.4)$$

where $\langle N_{\text{cluster/vdM}} \rangle$ is the mean number of pixel cluster at the peak of the scan and $\mathcal{L}_{\text{ins/vdM}}$ is the instantaneous luminosity obtained in the scan [23].

3.2 Cluster coincidence algorithm

The other object used by the TEPX luminometer to measure the event rate are two-fold coincidences. Coincidences are less prone to contamination by false hits produced in the detector after a bunch crossing (afterglow), due to the slow dissipation of charge and neutrons produced by the surrounding material (albedo). Two-fold coincidences are created when a particle hits overlapping modules, in the different layers of the TEPX disks. Due to this, coincidences are more likely to be a real hit than random electrical noise. The cylinder/disk like geometry of the TEPX detector allows for coincidences to be constructed in two ways: coincidences in ϕ require modules overlapping in the same ring, in front and

in the back of a double sided disk, while coincidences in r requires overlapping modules from different layers. These two ways of constructing two-fold coincidences are illustrated in Figure 3.2. The surface area of overlapping modules tends to be larger in ϕ than in the r direction. In order for a 2x coincidence to be considered, activated pixel clusters must fall in to specific cuts (on their δr and $\delta\phi$ separations). Finally, three-fold coincidences can occur as well, however, these types of coincidences are beyond the scope of this work. Coincidences provide another method of measuring luminosity and bring more stability, linearity and precision to the TEPX luminometers.

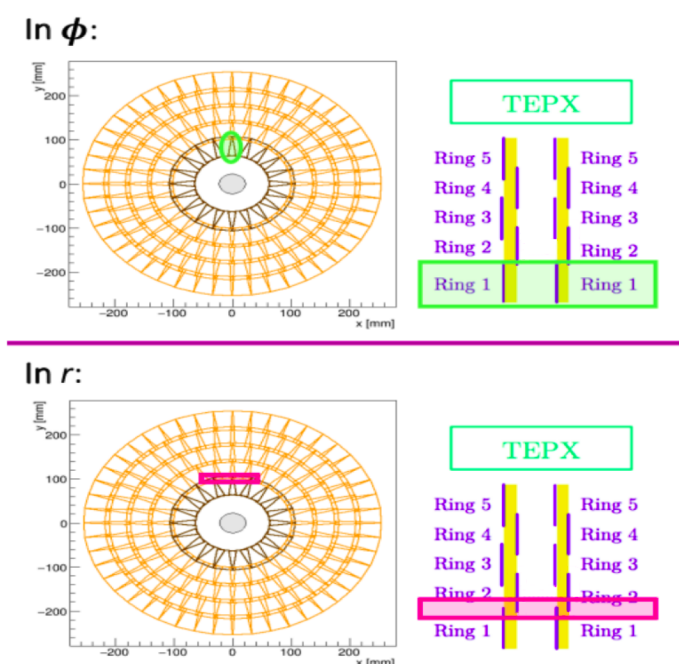


Fig. 3.2 Diagram of the regions in r and ϕ where pixel modules overlap, between the front and the back layers of one double-sided disk, from which two-fold coincidences come.

3.3 Calibration using the van der Meer method

The calibration of the luminometers is done by performing van der Meer scans, where the goal is to determine the calibration constant σ_{vis} .

In practice, the normalized bunch transverse distributions of each beam is not known, thus the overlap width integrals in 1.4 cannot be solved analytically. The vdM scans determines the valued of these integrals by separating the two beams and moving them across each

other while measuring the resulting rates (Figure 3.3 (left) illustrates this process)

$$\int \rho_1(x)\rho_2(x)dx = \frac{R_x(0)}{\int R_x(\Delta x)d\Delta x} \quad (3.5)$$

where $R_x(\Delta x)$ is the measured rate, when the beams are separated a distance Δx . Defining the beam overlap width as

$$\Sigma_x = \frac{1}{\sqrt{2\pi}} \frac{\int R_x(\Delta x)d\Delta x}{R_x(0)} \quad (3.6)$$

doing the same can be done for Σ_y , equation 1.4 can be rewritten:

$$\mathcal{L} = \frac{N_1 N_2 N_p f}{2\pi \Sigma_x \Sigma_y} \quad (3.7)$$

Once measurements have been taken, the rate is plotted as a function of beam separation and a Gaussian-like function is fitted to the data, as shown in Figure 3.3 (right). Using this function, the integral in equation 3.6 can be solved and the overlap width determined. Using 1.1 and 1.4 the calibration constant σ_{vis} can be determined:

$$\sigma_{vis} = \frac{2\pi \Sigma_x \Sigma_y}{N_1 N_2 N_p f} R_{peak} \quad (3.8)$$

where R_{peak} is the measured rate at the peak of the scan [24][23]. The original procedure can be found in [25].

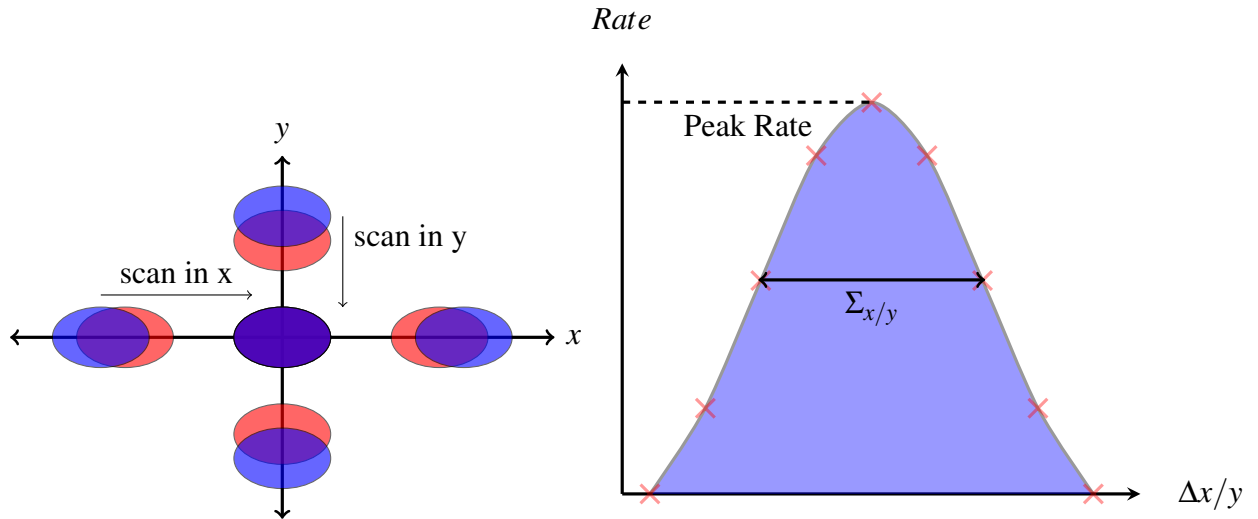


Fig. 3.3 *Left*: A diagram that shows how the two beams are scanned across the x and y axis. *Right*: An example of a Gaussian-like function (Blue), being fitted to the rate measurements (red xs) taken during a VDM scan.

3.4 Data acquisition

After event rate measurements have been taken, the data needs to be safely transferred and stored. In order to do this, several systems are put in place. Every subdetector has a dedicated CMS subsystem or a dedicated BRIL (Beam Radiation, Instrumentation, and Luminosity) system that takes care of this process. In the case of the TEPX, and other luminometers described in section 3.4.1, a combination of CMS and BRIL systems will be used, while TEPXD4R1 will be solely operated by BRIL.

The way counts per bunch crossing measured by a given luminometer are stored in CMS, is by using histograms. Every time a full orbit of bunches collides (3564 bunches), the counts per bunch crossing is histogrammed and stored. Depending on the geometry of the subdetector, the number of histograms generated by each changes. In the case of TEPX and TEPXD4R1 a histogram is created per quarter ring, this means that a total of 152 histograms are created by TEPX (not including the histograms from D4R1) and 8 by TEPXD4R1, in one orbit. The histogramming is done by the dedicated back-end of each subdetector, a combination of software and hardware components in charge of creating these histograms. Once the histograms have been correctly created they are read, processed and stored by the BRILDAQ (BRIL data acquisition) system. Figure 3.4 shows an example of a histograms for TEPX in the case of pixel clusters.

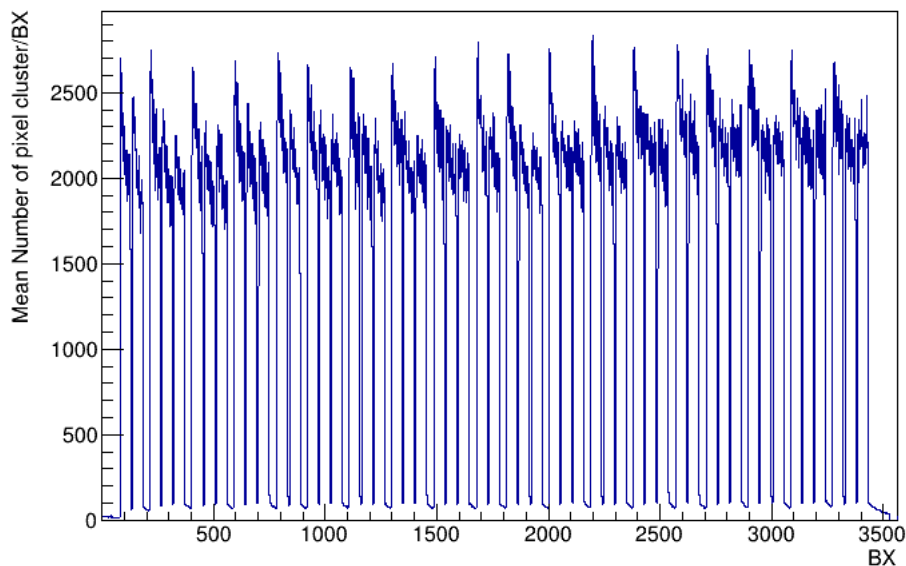


Fig. 3.4 The histogram shows the mean number of pixel clusters per bunch crossing (BX) for one lumisection (23.3 seconds), measured by the Phase-1 pixel detector during regular physics runs. The measurements from the 2018 data taking period.

Once histograms have been created, safely transferring and storing them is important, in order to do this the memory required to store them needs to be known. The memory size of each histogram depends on the information in each of them. All histograms have 3564 bins, one bin for each bunch crossing, these bins store the number of counts measured in a given bunch crossing, thus, the bits of information stored in these bins will give the memory of each histogram.

$$\text{Memory per Hist} = \text{No. of Bins} \times \text{bits per Bin} \quad (3.9)$$

where the bits per Bin are calculated using

$$\text{bits per Bin} = \log_2(N) \quad (3.10)$$

where N is the maximum expected number of counts per bunch crossing for a given integration period, it is worth mentioning that the results from equation 3.10 are rounded up to the closes integer. The maximum expected number of counts per bunch crossing is given by

$$N = n \frac{\text{Total Trigger Rate}}{3564} t \quad (3.11)$$

where n is the mean number of counts per event and t is the integration period. Equation 3.11 assumes that the Total Trigger Rate is distributed uniformly. Once the memory of the histogram is known, the data bandwidth needed to store all the histograms can be calculated, the Data Transfer Rate is given by

$$\text{Data Transfer Rate} = \frac{\text{No.Hist} \times \text{MemoryperHist}}{t} \quad (3.12)$$

where No. Hist is the number of histograms created by the detector and t is the time in which the information is transferred.

32-bit word implementation

The data at CMS is not transferred bit by bit, rather, is transferred in packages of information called words. Each word contains 32-bits of information, this means that all data transferred has to, first, be converted in to a 32-bit word. The way this is applied to the histograms is by converting the information in each bin in to a word, this is done in two ways:

- If the Bits per bin ≤ 16 bits, the number of bits is rounded to 16 and two bins are grouped in one word.
- If $16 \leq \text{Bits per bin} \leq 32$, the number of bits is rounded to 32-bit word and one word is used for each bin.

Aside from this, the TEPX luminometers use additional words for the overhead of the histograms data format:

- 9 words for the header for TEPX and D4R1.
- 768 words for errors for TEPX and 160 for D4R1.
- 4 words for the mask for TEPX and 2 for D4R1.

These additional data has to be taken in to account for each histograms, when calculating the needed memory to store and transfer them. Finally, using equation 3.10 the bits per bin can be calculated, using data from the high pileup simulation [26]. The results for the TEPX luminometers is shown in Table 3.1. Using this and equation 3.12, the data rates

Table 3.1 Table shows the Trigger rate (kHz), counts per event per detector unit (histogram), number of counts per bx per integration period (1s) and the memory bits required per histogram bin.

	Trigger rate (kHz)	Counts per event	Counts/bx/1s	Bits/bin
TEPXD4R1 Clusters	825	539	1.25e+05	17
TEPXD4R1 2x Coincidences	825	54	1.25e+04	14
TEPX Clusters	75	539	1.13e+04	14
TEPX 2x Coincidences	75	54	1.14e+03	11

can be calculated, the results are shown in Table 3.2 for a transferring time of 1 s.

Table 3.2 Data transfer rates for the TEPX luminometers for pileup 200. Columns shown are number of histograms, memory per histogram and data transfer rates (Mbps) for an integration period of 1s.

	Number of Histograms	Memory per histogram (Kb)	Data Transfer Rates (Mbps)
TEPXD4R1 Clusters	8	124	0.95
TEPXD4R1 2x Coincidences	8	67	0.5
TEPX Clusters	152	82	12.5
TEPX 2x Coincidences	152	82	12.5

3.4.1 Other luminometers

The TEPX luminometer is not the only luminometer of the CMS Phase-2 detector, each layer of the detector will have a dedicated luminometer, and corresponding algorithm, to

ensure the best luminosity measurements possible. Figure 3.5 shows the location of the different luminometers at the CMS detector, for the Phase-2 upgrade. A brief description of the luminometers is presented below.

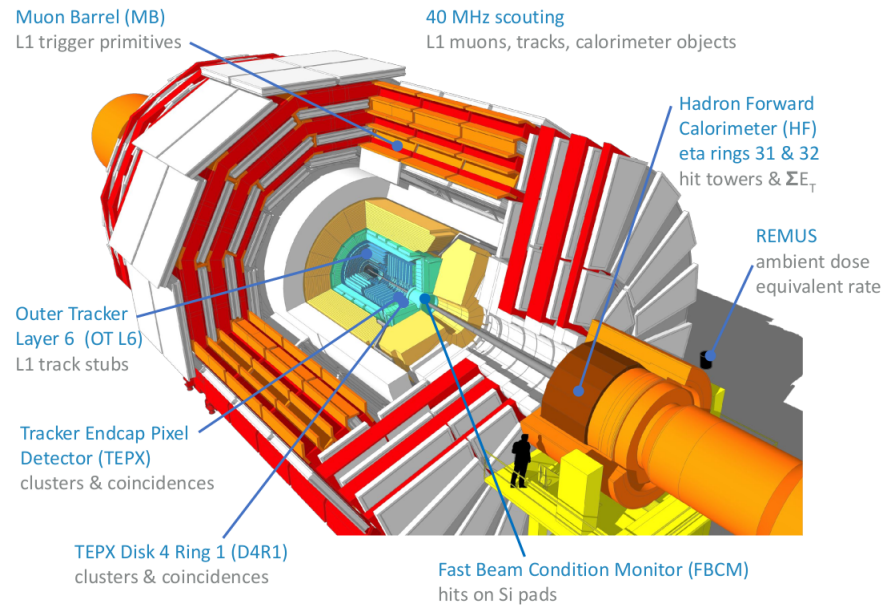


Fig. 3.5 Layout of the different subsystems and luminometers at CMS.

Outer tracker layer 6

From the outer tracker (OT), layer 6 will be a designated luminometer. The object used by these luminometer are track stubs, which are two-hit coincidences between closely spaced silicon modules. Figure 3.6 show the layout of the new Phase-2 outer tracker, layer 6 is located in the outer tracker barrel, specifically, the TB2S section.

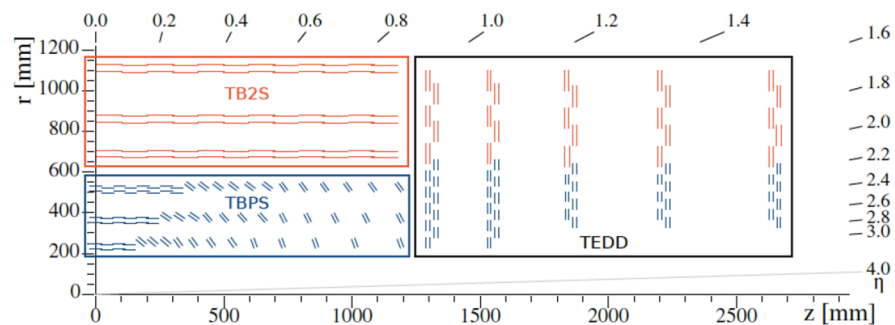


Fig. 3.6 Diagram of the different parts that conform the outer tracker, the two barrel regions, TBPS and TB2S, and the end-cap region TEDD. The OT layer 6 luminometer corresponds to the last upper layer of TB2S.

Layer 6 consists of 76 ladders of 12 strip modules made of two Si-strip sensors, as shown in Figure 3.7 (left). The ladders span fully, in the azimuthal range, at each end of the CMS detector. The reconstruction method of the track stubs is shown in Figure 3.7 (right) as well. The tracks are reconstructed at 40 MHz.

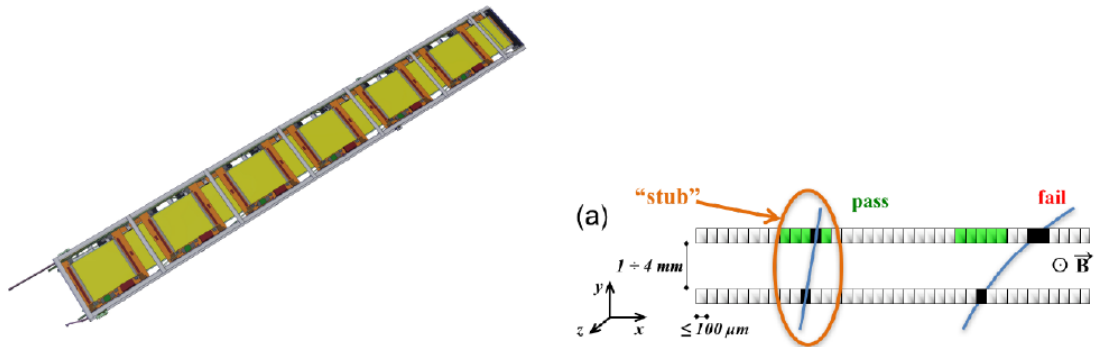


Fig. 3.7 *Left*: An example of a ladder with the the 12 strip modules (regions in yellow). *Right*: Diagram of the stub selection process. The black squares represent hits, and the green squares represent the regions where the other hit could take place, to be considered a stub.

The OT layer 6 luminometers, creates one histograms per one 12 module ladder, for a total of 152. As well as the TEPX luminometers, the histograms created in layer 6 will have additional words for the overhead of the histograms data format:

- 9 words for the header.
- 192 words for errors.
- 4 words for the mask.

Figure 3.8 shows the expected number of track stubs per bunch crossing as function of the ladders ID. Tables 3.3 and 3.4 show the expected Bits per Bin and the Data Transfer Rates for the OT layer 6 luminometer, calculated using data from the high pileup simulation.

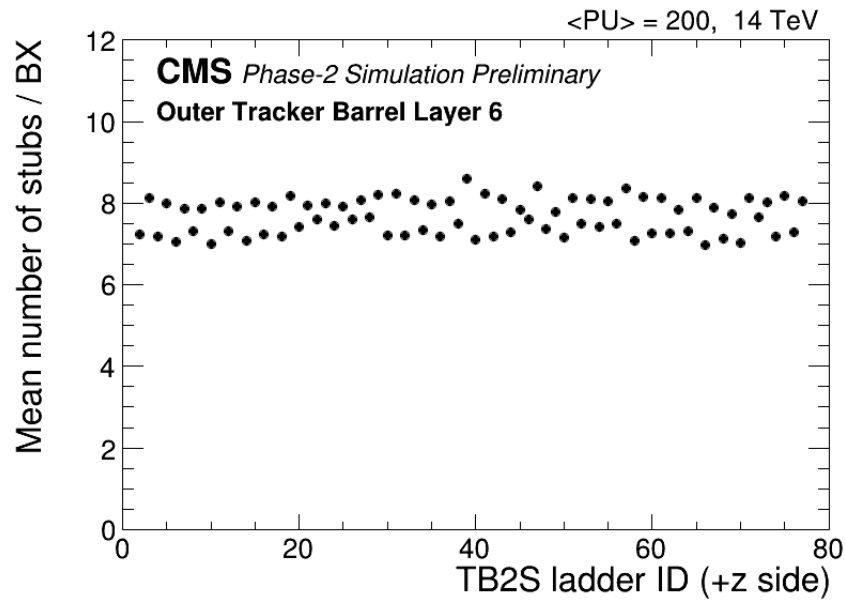


Fig. 3.8 Simulated expected number of stubs per ladder per event as a function of ladder ID.

Muon drift tube

The muon DT luminometer follows the same design described in section 2.2. The entire DT system is formed by 250 gas chambers, installed in the barrel yoke of the CMS detector, as shown in Figure 2.5. The chambers are distributed across 5 wheels labeled YB0, YB \pm 1 and YB \pm 2, four radial stations, MB1-MB4, and 12 ϕ sectors [27].

The objects used by this luminometer are called trigger primitives, which are reconstructed muon track segments per DT chamber. The tracks are reconstructed at a trigger frequency of 40 MHz, using hits from the DT and RPC detectors. The rate of trigger primitives has been studied and extrapolated to the expected instantaneous luminosity of the HL-LHC, $7.5 \times 10^{34} \text{ cm}^{-2} \text{ s}^{-1}$, using the data from Run 2. Figure 3.9 shows the expected rates for the YB0 and YB+2 wheels. The large difference on the measured rate, between the MB1 and the rest of the chambers in the MB2 and MB3 stations, is due to a significant contribution of particle from punch-through jets.

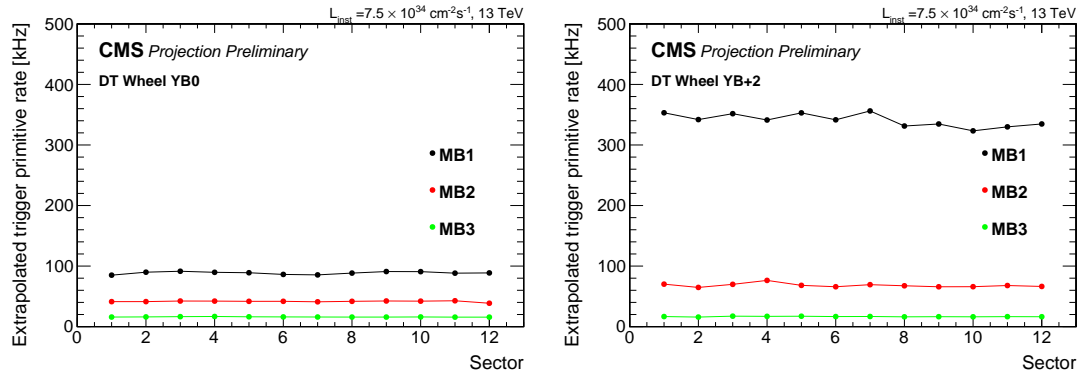


Fig. 3.9 Expected rates of trigger primitives per DT chamber for the YB0 (left) and YB+2 (right) wheels.

The DT luminometer will create one histogram per DT chamber, giving a total of 250 histograms. Tables 3.3 and 3.4 show the expected Bits per Bin and the Data Transfer Rates for the DT luminometer, using extrapolated data from the 2018 data taking period.

BM TF

The Barrel Muon Track Finder (BM TF) is an algorithm that uses reconstructed muon tracks to provide luminosity measurements. As its name suggests, The algorithm uses information from all the DT and RPC gas chambers, located in the barrel of the muon system, to reconstruct muon tracks. One histograms is created by the algorithm. Tables 3.3 and 3.4 show the expected Bits per Bin and the Data Transfer Rates for the BM TF algorithm [28]. As well as the DT luminometer, BTMS uses extrapolated data from the 2018 data taking period.

3.4.2 Data transfer rates for all luminometers

Using the number of histograms, as well as the mean number of counts per event for each luminometer [26], the number of Bits per Bin as well as the Data Transfer Rates can be calculated for all luminometers. This is shown in Tables 3.3 and 3.4 respectively.

Table 3.3 Trigger rate (kHz), counts per event per detector unit (histogram), number of counts per bx per integration period (1s) and the memory bits required per histogram bin.

	Trigger rate (kHz)	Counts per event	Counts/bx/1s	Bits/bin
TEPXD4R1 Clusters	825	539	1.25e+05	17
TEPXD4R1 2x Coincidences	825	54	1.25e+04	14
TEPX Clusters	75	539	1.13e+04	14
TEPX 2x Coincidences	75	54	1.14e+03	11
OT Layer 6 track stubs	40000	8	8.98e+04	17
DT Trigger Primitives	40000	0.0125	140	8
BMTF Tracks	40000	0.041	460	9

Table 3.4 Data transfer rates for the different luminometers for pileup 200. Columns shown are number of histograms, memory per histogram and data transfer rates (Mbps) for an integration period of 1s.

	Number of Histograms	Memory per histogram (Kb)	Data Transfer Rates (Mbps)
TEPXD4R1 Clusters	8	124	0.95
TEPXD4R1 2x Coincidences	8	67	0.5
TEPX Clusters	152	82	12.5
TEPX 2x Coincidences	152	82	12.5
OT Layer 6 track stubs	152	120	18.3
DT Trigger Primitives	250	28	7.13
BMTF Track	1	57	0.057

From these tables it can be concluded that the minimum bandwidth required will be 18.3 Mbps, corresponding to the OT luminometer. The total storage needed per day for all luminometers presented here can be calculated, assuming an operation time of 12 hours, the total storage needed will be 280.46 GB. Since other luminometers will be in operation, besides the ones discussed here, 280.46 GB is the minimum storage per day required to ensure no data is lost.

Chapter 4

Analysis and Results

4.1 Linearity of the TEPX luminometers

The linearity of the detector is an important parameter. The determination of the calibration constants is done by performing a vdm scan, however, vdm scans are performed at considerably low pileup, $\mu = 0.5$, and it is then extrapolated to a pileup of ≈ 200 , this extrapolation generates a significant source of uncertainty. An ideal detector will demonstrate a linear relation between the measured event rate, and the instantaneous luminosity. This also implies a linear relation between the event rate and the pileup:

$$\langle N_{\text{clusters/int}} \rangle = \frac{\langle N_{\text{cluster}} \rangle}{\mu} = \frac{\sigma_{\text{vis}}}{\sigma_{\text{tot}}} \quad (4.1)$$

$$\langle N_{\text{clusters}} \rangle = \frac{\sigma_{\text{vis}}}{\sigma_{\text{tot}}} \mu \quad (4.2)$$

Different sources can affect the linearity of a detector, such as, efficiency factors depending on single bunch instantaneous luminosity, short-term effects, like overall rate-dependent efficiency factors, out-of-time effects due to late arriving particles, etc. At CMS, the monitoring and corrections to linearity are performed using emittance scans [24]. Emittance scans are used to correct the measured event rate in each fill, for efficiency and linearity.

As mentioned before, the TEPX luminometers use two different observables when measuring the event rate, pixel clusters and two-fold coincidences. A linear response from the TEPX and TEPXD4R1 luminometers is a must, for a precise luminosity measurement. To see the response of the luminometers, the number of clusters/coincidences per event is histogrammed, using data from the high pileup simulation, this is done for each ring and disk of the luminometer. In the case of coincidences in r, the histograms are created

per set of rings. Once the distribution for each histogram is obtained, the mean of these distributions is plotted as a function of pileup. A line is fitted to the lowest pileup values, from 0 to 2, to simulate vdm scan conditions. This line is then extrapolated up to a pileup of 200. Figures 4.1-4.4 show these fits, where the deviations from the straight line are found to be less than 1%. The linearity of the detector was the main source of uncertainty during Run 2, however, this is not the only one, other sources include afterglow, x-y nonfactorization, cross-detector consistency, etc, but these types of uncertainties can only be estimated during regular physics runs [24].

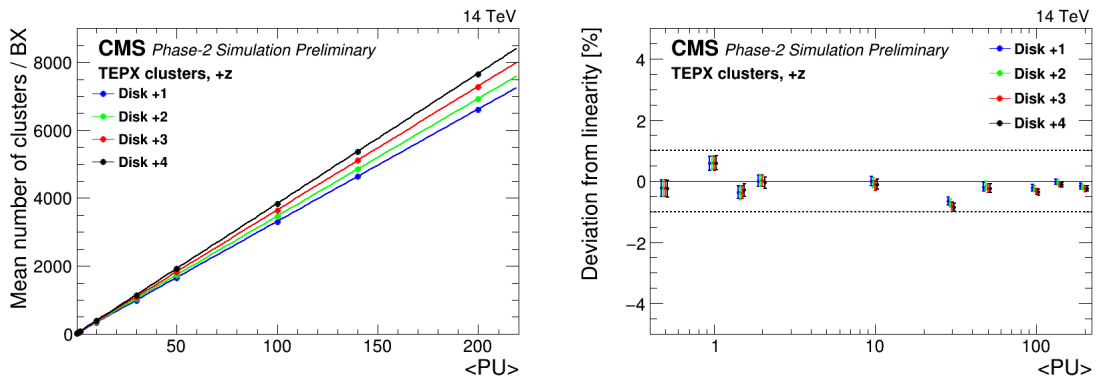


Fig. 4.1 *Left*: Simulated mean number of pixel cluster per bx for the each disk of TEPX, as a function of pileup. A line is fitted between the pileup values of 0 and 2, and the extrapolated to higher pileup values. *Right*: Deviation from linearity for clusters for TEPX. The nonlinearity is calculated as the relative difference between the points and the fitted function.

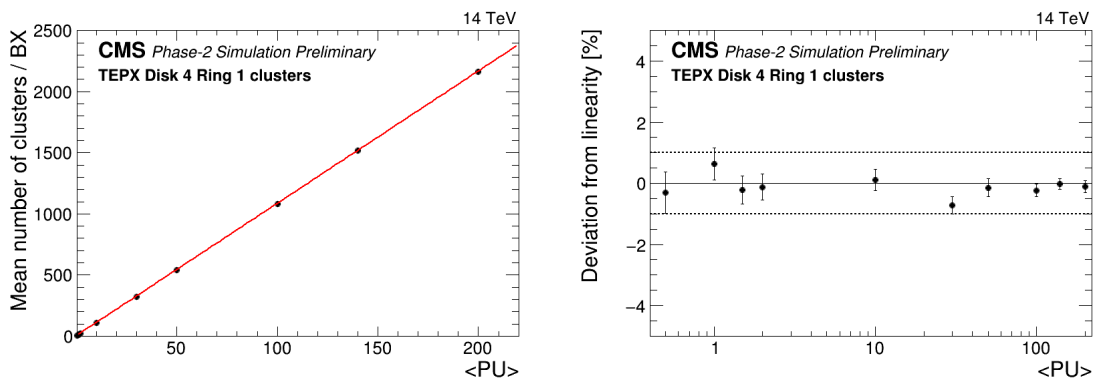


Fig. 4.2 *Left*: Simulated mean number of pixel cluster per bx for the entirety of TEPXD4R1, as a function of pileup. A line is fitted between the pileup values of 0 and 2, and the extrapolated to higher pileup values. *Right*: Deviation from linearity for clusters for TEPXD4R1. The nonlinearity is calculated as the relative difference between the points and the fitted function.

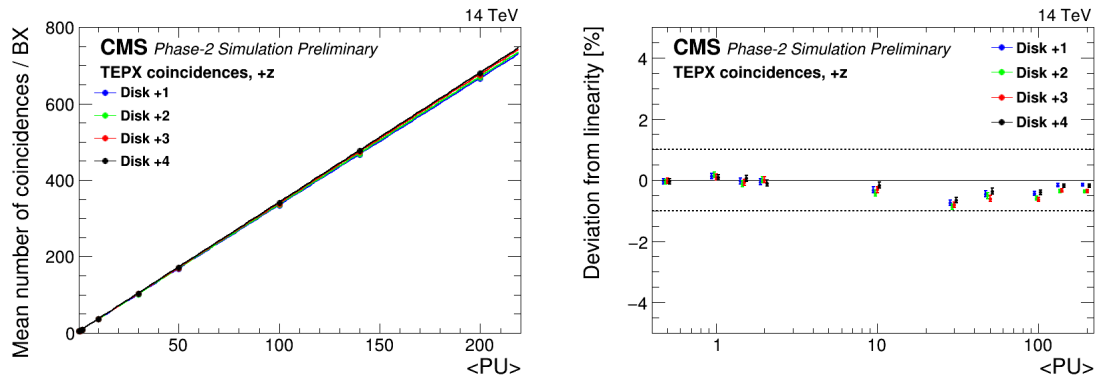


Fig. 4.3 *Left*: Simulated mean number of two-fold coincidences per bx for the each disk of TEPX, as a function of pileup. A line is fitted between the pileup values of 0 and 2, and the extrapolated to higher pileup values. *Right*: Deviation from linearity for clusters for TEPX. The nonlinearity is calculated as the relative difference between the points and the fitted function.

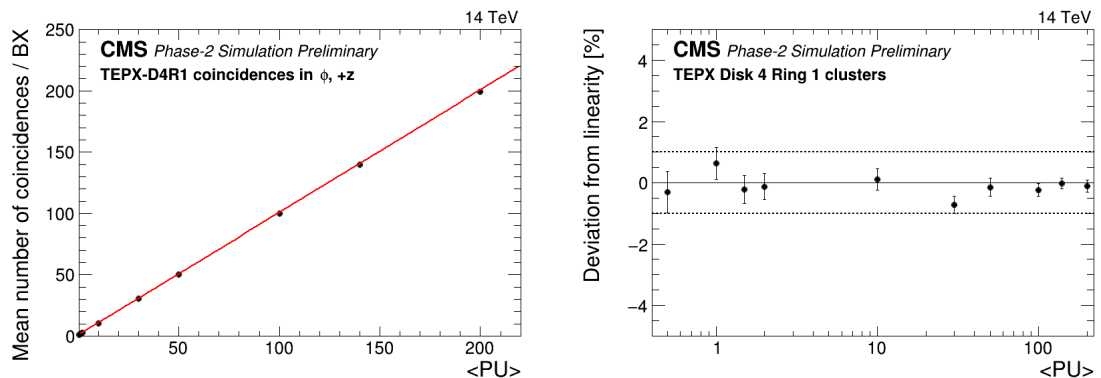


Fig. 4.4 *Left*: Simulated mean number of two-fold coincidences per bx for the entirety of TEPXD4R1, as a function of pileup. A line is fitted between the pileup values of 0 and 2, and the extrapolated to higher pileup values. *Right*: Deviation from linearity for clusters for TEPXD4R1. The nonlinearity is calculated as the relative difference between the points and the fitted function.

4.2 Statistical precision for Physics data taking

The statistical precision of the luminometers is a very important parameter, the precision at which the event rate is determined is another statistical uncertainty considered when calculating the luminosity. The goal for the HL-LHC is to achieve an accuracy of 1% for luminosity measurements, for this, a subpercentage precision is desired for all luminometers. The instantaneous luminosity expected for the HL-LHC is of $7.5 \times 10^{34} \text{ cm}^{-2}\text{s}^{-1}$, almost 4 times the luminosity reached during Run 2 of the LHC. This value of luminosity can only be achieved if the number of proton-proton interactions per bunch (pileup), is equal or close to 200, during regular physics runs.

The statistical precision of the TEPX and TEPXD4R1 luminometers was calculated using:

$$\text{Relative statistical precision}\% = 100 \times \frac{\sqrt{N}}{N} \quad (4.3)$$

where N is the mean number of pixel clusters/coincidences per event measured by the detector, for a given integration period, and is given by

$$N = (\text{Number of counts per event}) \times (\text{Trigger Frequency per bx}) \times (\text{Time integration period}) \quad (4.4)$$

the Trigger Frequency per bx is

$$\text{Trigger Frequency per bx} = \frac{\text{Total Readout Frequency}}{\text{Total Number of bx (3564)}} \quad (4.5)$$

Assuming total readout frequency is uniformly distributed across all bunch crossings.

During regular physics runs, the TEPXD4R1 luminometer will run at a Total Readout Frequency of 825kHz, while the TEPX luminometer will run at 75kHz. The Number of counts per event is taken from simulated measurements using Run 2 data, specifically from the 2018 data taking period. The statistical precision of the TEPX luminometers, for pixel clusters and two-fold coincidences (2x coincidences), is shown in Table 4.1.

Table 4.1 Statistical precision of the TEPX luminometers in % for pileup 200. Columns shown are the luminometer readout frequency, and estimated precision for 1 bunch crossing and 2748 colliding bunches for integrated of 1s.

	Readout Frequency (kHz)	1 bx, 1s	2748 bx, 1s
TEPXD4R1 Clusters	825	0.1	0.0019
TEPXD4R1 2x Coincidences	825	0.31	0.006
TEPX Clusters	75	0.095	0.0018
TEPX 2x Coincidences	75	0.34	0.0066

4.3 Statistical precision for vdM

The vdM scan is performed under special conditions, in order to determine the calibration constant σ_{vis} as accurately as possible. The scan is performed at a low pileup of 0.5, this is done since the specific precision needed to determine σ_{vis} cannot be reached during regular physics runs with higher pileup. Once σ_{vis} is determined, it can be used during regular physics runs, this is because the detector's acceptance should not change under either of the two conditions.

The scan's duration is of 30 seconds per step, in which event rate measurements are taken. The precision at which these measurements are taken, will determine the precision with which the calibration constant is determined, among other things. The statistical precision for event rates during a vdM scan is calculated with equation 4.3, using the same data used for physics runs. To simulate the lower pileup, the mean number of clusters/coincidences per event is divided by 400, since that data corresponds to a pileup of 200. During vdM scans the TEPX and TEPXD4R1 will run at a higher trigger frequency of 1MHz and 2 MHz respectively. This is to make up for the low event rates due to the low amount of interaction. Table 4.2 shows the statistical precision for different numbers of bunches as well as different integration periods.

Table 4.2 Statistical precision of the TEPX luminometers in % for pileup 0.5. Columns shown are the luminometer readout frequency, estimated precision for 1bx per 1 s integration, and 1 and 150 bx for 30 s integration period.

	Readout Frequency (kHz)	1 bx, 1s	1 bx, 30s	150 bx, 30s
TEPXD4R1 Clusters	2000	1.3	0.23	0.019
TEPXD4R1 2x Coincidences	2000	4.07	0.74	0.060
TEPX Clusters	1000	0.52	0.095	0.0077
TEPX 2x Coincidences	1000	1.9	0.34	0.028

4.3.1 Toy simulation of the vdM scan

Using the results from the previous section a vdm scan toy study was created to calculate the statistical uncertainty for σ_{vis} . To simulate the event rate measurements, a Gaussian distribution is used:

$$R(\Delta x) = N_0 e^{-\frac{(\Delta x - x_0)^2}{2\Sigma_x^2}} \quad (4.6)$$

where $R(\Delta x)$ is the measured event rate, Δx is the beam separation in the x axis, N_0 is the mean number of cluster/coincidences per event for 1 bx in a 30 s integration period and Σ_x is the beam overlap width. The toy study simulates 25 steps for the vdM scan, that is, 25 event rate measurements, and uses a beam overlap width of $\Sigma_x = 120$ mm. The statistical

uncertainty for each measurement was calculated using

$$\text{statistical uncertainty} = \sqrt{R(\Delta x)} \quad (4.7)$$

Once the measurements have been histogrammed as a function of beam separation Δx , another Gaussian distribution is fitted to the measurements to simulate vdM scan process for determining σ_{vis} . Figures 4.5 and 4.6 show the results of this process for TEPX and TEPXD4R1 luminometers for pixel cluster and coincidences.

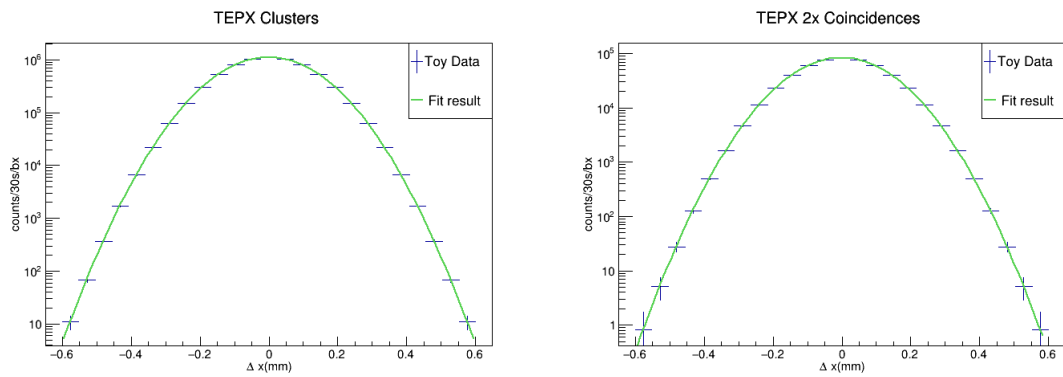


Fig. 4.5 Simulated rate measurements for pixel clusters (Left), coincidences (Right), and their corresponding uncertainties (blue lines) for TEPX, during a vdM scan. The green line corresponds to the fitted Gaussian distribution.

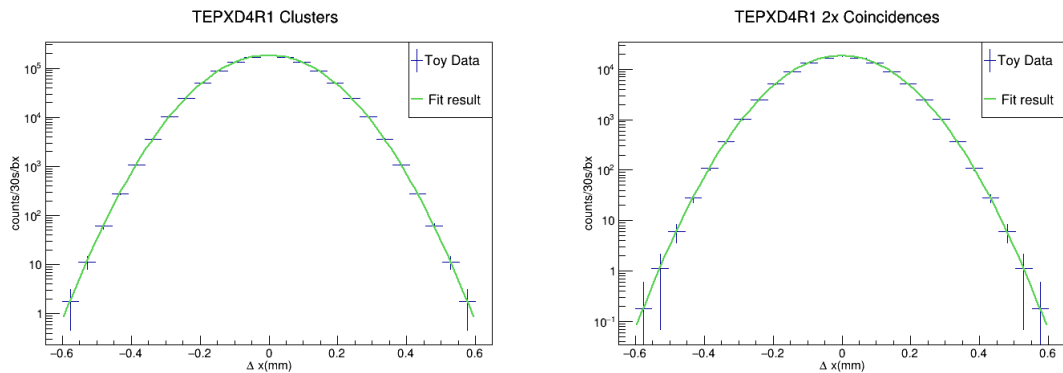


Fig. 4.6 Simulated rate measurements for pixel clusters (Left), coincidences (Right), and their corresponding uncertainties (blue lines) for TEPXD4R1, during a vdM scan. The green line corresponds to the fitted Gaussian distribution.

Once the histograms is fitted with a Gaussian distribution, the mean number of counts per event N_0 , the beam overlap width Σ and their corresponding uncertainties, δN_0 and $\delta \Sigma_x$, are extracted from the fit. The two sources of statistical uncertainty for σ_{vis} , from the vdM scan, come from two variables: the beam overlap with Σ_x and the mean number of counts per event N_0 . In order to calculate the uncertainty for the calibration constant, it will first need to be seen if any correlations exist between these variables. This is done by extracting the correlation matrices form the fit. In the case of TEPX, for pixel cluster, the correlation matrix is:

$$cor = \begin{bmatrix} \rho_{N_0, N_0} & \rho_{N_0, x_0} & \rho_{N_0, \Sigma_x} \\ \rho_{x_0, N_0} & \rho_{x_0, x_0} & \rho_{x_0, \Sigma_x} \\ \rho_{\Sigma_x, N_0} & \rho_{\Sigma_x, x_0} & \rho_{\Sigma_x, \Sigma_x} \end{bmatrix} = \begin{bmatrix} 1 & 0 & -0.5774 \\ 0 & 0 & 0 \\ -0.5774 & 0 & 1 \end{bmatrix} \quad (4.8)$$

a similar correlation of ≈ -0.5 can be found for TEPX and D4R1 luminometers. Since as significant correlation exists between N_0 and Σ_x , this will have to be taken in to account, when calculating the statistical uncertainty of σ_{vis} . Thus, the relative uncertainty will be given by the equation

$$\frac{\delta \sigma_{vis}}{\sigma_{vis}} = \frac{1}{\sigma_{vis}} \sqrt{\left(\frac{d\sigma_{vis}}{dN_0} \delta N_0 \right)^2 + \left(\frac{d\sigma_{vis}}{d\Sigma_{x/y}} \delta \Sigma_{x/y} \right)^2 + \left(2 \frac{d\sigma_{vis}}{dN_0} \frac{d\sigma_{vis}}{d\Sigma_{x/y}} cov(N_0, \Sigma_{x/y}) \right)} \quad (4.9)$$

where $\delta \sigma_{vis}$ is the statistical uncertainty of σ_{vis} and $cov(N_0, \Sigma_{x/y})$ is the $N_0, \Sigma_{x/y}$ element of the covariance matrix, which along with the correlation matrix, is extracted form the fit. It is worth mentioning, that equation 4.9 assumes that no correlation exist between Σ_x and Σ_y . To calculate the derivatives of σ_{vis} an approximation is made

$$\sigma_{vis} \approx N_0 \Sigma_x \Sigma_y \quad (4.10)$$

In here, the constant terms like the frequency f , the bunches intensities N_1 and N_2 as well as the number of bunches N_b are not taken in to account, since these terms will cancel out when calculating $\delta \sigma_{vis} / \sigma_{vis}$. Finally, calculating the derivatives of 4.10 and using them on 4.9 gives

$$\frac{\delta \sigma_{vis}}{\sigma_{vis}} = \sqrt{\left(\frac{\delta N_0^2}{N_0} \right) + \left(2 \frac{\delta \Sigma^2}{\Sigma} \right) + \left(\frac{4 cov(N_0, \Sigma)}{N_0 \Sigma} \right)} \quad (4.11)$$

Equation 4.11 assumes that $\Sigma_x = \Sigma_y$, hence

$$\left(\frac{\delta \Sigma_x^2}{\Sigma_x} \right) + \left(\frac{\delta \Sigma_y^2}{\Sigma_y} \right) = \left(2 \frac{\delta \Sigma^2}{\Sigma} \right)$$

$$\left(\frac{2cov(N_0, \Sigma_x)}{N_0 \Sigma_x}\right) + \left(\frac{2cov(N_0, \Sigma_y)}{N_0 \Sigma_y}\right) = \left(\frac{4cov(N_0, \Sigma)}{N_0 \Sigma}\right)$$

Using equation 4.11, the relative uncertainty for σ_{vis} is calculated for 1 and 150 bunches for a 30 s integration period, Table 4.3 shows the result:

Table 4.3 Results from the vdM toy study for 1 bx and 150 bx: Table shows mean number of cluster/coincidences per event (N_0), beam overlap widths (Σ) and the uncertainties for mean number of cluster/coincidences per event (δN_0), beam overlap widths ($\delta \Sigma$) and σ_{vis} ($\delta \sigma_{vis}/\sigma_{vis}(\%)$) for Phase II luminometers.

	N_0	δN_0	Σ	$\delta \Sigma$	$\delta \sigma_{vis}/\sigma_{vis}(\%)$	$\delta \sigma_{vis}/\sigma_{vis}(\%), 150 \text{ bx}$
TEPXD4R1 Clusters	181000	210	0.12	0.00008	0.066	0.0054
TEPXD4R1 2x Coincidences	18100	66	0.12	0.00025	0.21	0.017
TEPX Clusters	1.1e+06	510	0.12	0.00003	0.027	0.0022
TEPX 2x Coincidences	82900	140	0.12	0.00012	0.098	0.008

4.4 Comparison to other luminometers

Applying the same methods described above, but utilizing the different objects for each luminometer (track stubs, trigger primitives and muon tracks), the statistical uncertainty for vdM and physics runs conditions can be calculated using data extrapolated from the 2018 taking period [29] for DT and BMTF, and data from the high pile up simulation for TEPX and OT. This is shown in Tables 4.4 and 4.5, while Table 4.6 shows the relative statistical uncertainty for σ_{vis} for all luminometers.

Table 4.4 Statistical precision in % for pileup 200. Columns shown are the luminometer readout frequency, and estimated precision for 1 bx and 2748 bx for integrated of 1s.

	Readout Frequency (kHz)	1 bx, 1s	2748 bx, 1s
TEPXD4R1 Clusters	825	0.1	0.0019
TEPXD4R1 2x Coincidences	825	0.31	0.0060
TEPX Clusters	75	0.095	0.0018
TEPX 2x Coincidences	75	0.34	0.0066
OT Layer 6 track stubs	40000	0.028	0.00054
DT Trigger Primitives	40000	1.21	0.023
BMTF	40000	4.61	0.0879

Table 4.5 Statistical precision in % for pileup 0.5. Columns shown are the luminometer readout frequency, estimated precision for 1bx per 1 s integration, and 1 and 150 bx for 30 s integration period.

	Readout Frequency (kHz)	1 bx, 1s	1 bx, 30s	150 bx, 30s
TEPXD4R1 Clusters	2000	1.3	0.23	0.019
TEPXD4R1 2x Coincidences	2000	4.07	0.74	0.06
TEPX Clusters	1000	0.52	0.095	0.0077
TEPX 2x Coincidences	1000	1.9	0.34	0.028
OT Layer 6 track stubs	40000	0.57	0.1	0.0085
DT Trigger Primitives	40000	24.2	4.4	0.36
BMTF	40000	92.1	16.8	1.3

Table 4.6 Results from the vdM toy study for 1 bx and 150 bx: Table shows normalizations (N_0), beam widths (Σ) and the uncertainties for normalizations (δN_0), beam widths ($\delta \Sigma$) and σ_{vis} ($\delta \sigma_{vis}/\sigma_{vis}\%$) for Phase II luminometers.

	N_0	δN_0	Σ	$\delta \Sigma$	$\delta \sigma_{vis}/\sigma_{vis}(\%)$	$\delta \sigma_{vis}/\sigma_{vis}(\%), 150 \text{ bx}$
TEPXD4R1 Clusters	181000	210	0.12	0.00008	0.066	0.0054
TEPXD4R1 2x Coincidences	18100	66	0.12	0.00025	0.21	0.017
TEPX Clusters	1.1e+06	510	0.12	0.00003	0.027	0.0022
TEPX 2x Coincidences	82900	140	0.12	0.00012	0.098	0.008
OT Layer 6	907000	470	0.12	0.00004	0.03	0.0024
DT	513	11	0.12	0.00150	1.2	0.1
BMTF	35.4	2.9	0.12	0.00571	4.7	0.39

Chapter 5

Conclusion and Summary

With the new luminosity goal of the HL-LHC, the CMS detector will receive several upgrades, in order to keep up with the new luminosity demands. These upgrades will come to several systems, which includes various subdetectors and luminometers. One of these subdetectors TEPX, will perform luminosity measurements with high statistics. One of its rings, TEPXD4R1, will perform luminosity measurements only. The TEPX will be operated by BRIL, utilizing the pixel cluster counting (PCC) method, as the main source of luminosity measurements.

The PCC algorithm will take advantage of the low occupancy and the 800 million pixels distributed across the 2 m^2 of the TEPX luminometer, to provide precise luminosity measurements. The TEPX luminometers will provide event rate measurements utilizing two types of objects: pixel clusters and two-fold coincidences.

In this work, the statistical precision of the TEPX luminometers, and other luminometers, is studied using simulated data. For physics runs (pileup of 200), the TEPX luminometers achieved a statistical precision per bunch per 1 s, below 0.1% for pixel clusters and below 0.4% for two-fold coincidences. In vdM conditions (pileup of 0.5), the precision is below 0.4% per bunch per 30 s, for pixel clusters and below 0.8% for coincidences. This translates to a precision under 0.1% per bunch for the calibration constant (σ_{vis}) for pixel clusters, and below 0.3% for coincidences. Both luminometers also achieve linearity deviations well below 1% up to a pileup of 200. These results show an excellent expected performance for TEPX luminometers, and in combination with the rest of the luminometers (OT layer 6, DT and BMTF), will provide precise luminosity measurements for the HL-LHC phase.

The network bandwidth and disk storage needed for the BRIL Phase 2 luminosity systems has been also estimated. Concluding that a bandwidth of at least 18.3 Mbps is required, and a disk storage of 280.46 GB per day is needed.

References

- [1] David J Griffiths. *Introduction to elementary particles; 2nd rev. version*. Physics textbook. Wiley, New York, NY, 2008. URL <https://cds.cern.ch/record/111880>.
- [2] Mark Thomson. *Modern particle physics*. Cambridge University Press, New York, 2013. ISBN 978-1-107-03426-6.
- [3] MissMJ. "Standard Model". URL https://en.wikipedia.org/wiki/Standard_Model#/media/File:Standard_Model_of_Elementary_Particles.svg.
- [4] CMS collaboration. "Observation of a new boson at a mass of 125 GeV with the CMS experiment at the LHC". *Physics Letters B*, 716(1):30 – 61, 2012. URL <https://doi.org/10.1016/j.physletb.2012.08.021>.
- [5] ATLAS collaboration. "Observation of a new particle in the search for the Standard Model Higgs boson with the ATLAS detector at the LHC". *Physics Letters B*, 716(1): 1 – 29, Sep 2012. URL <http://dx.doi.org/10.1016/j.physletb.2012.08.020>.
- [6] CMS collaboration. A measurement of the Higgs boson mass in the diphoton decay channel. *Physics Letters B*, 805:135425, 2020. ISSN 0370-2693. doi: <https://doi.org/10.1016/j.physletb.2020.135425>.
- [7] Official CERN web page. "DETECTOR". . URL <https://cms.cern/detector>.
- [8] Simon Mathieu White. *Determination of the Absolute Luminosity at the LHC*. PhD thesis, Orsay, Université Paris-Sud 11, 2010.
- [9] Michi Hostettler. LHC Luminosity Performance, May 2018. URL <https://cds.cern.ch/record/2319396>. Presented 21 Jun 2018.
- [10] Oliver Sim Brüning, Paul Collier, P Lebrun, Stephen Myers, Ranko Ostojic, John Poole, and Paul Proudlock. *"LHC Design Report"*. CERN Yellow Reports: Monographs. CERN, Geneva, 2004. doi: 10.5170/CERN-2004-003-V-1.
- [11] Official CERN web page. "Facts and figures about the LHC". . URL <https://home.cern/resources/faqs/facts-and-figures-about-lhc>.
- [12] Official CERN web page. "LHCb". . URL <https://home.cern/science/experiments/lhcb>.
- [13] Official CERN web page. "CMS". . URL <https://home.cern/science/experiments/cms>.
- [14] Corinne Pralavorio. "Final lap of the LHC track for protons in 2018". URL <https://home.cern/news/news/accelerators/final-lap-lhc-track-protons-2018>.

- [15] CMS collaboration. "CMS Physics: Technical design report volume 1: Detector performance and software". Report number: CERN-LHCC-2006-001. 2006. URL <http://cds.cern.ch/record/922757>.
- [16] W. Adam et al. The CMS Phase-1 Pixel Detector Upgrade. *JINST*, 16(02):P02027, 2021. doi: 10.1088/1748-0221/16/02/P02027.
- [17] D Contardo, M Klute, J Mans, L Silvestris, and J Butler. "Technical Proposal for the Phase-II Upgrade of the CMS Detector". Technical report, Geneva, Jun 2015. URL <https://cds.cern.ch/record/2020886>.
- [18] CMS collaboration. "The performance of the CMS muon detector in proton-proton collisions at $\sqrt{s}=7$ TeV at the LHC". *Journal of Instrumentation*, Volume 8, November 2013. URL <http://dx.doi.org/10.1088/1748-0221/8/11/P11002>.
- [19] G. Apollinari et. al. "High-Luminosity Large Hadron Collider (HL-LHC) Technical Design Report V. 0.1". Report number: CERN-2017-007-M. *CERN Yellow Reports: Monographs Archives Vol 4 (2017)*, 2017. URL <http://dx.doi.org/10.23731/CYRM-2017-004>.
- [20] Official CERN web page. "Project Schedule". . URL <https://project-hl-lhc-industry.web.cern.ch/content/project-schedule>.
- [21] "The Phase-2 Upgrade of the CMS Tracker". Technical report, CERN, Geneva, Jun 2017. URL <https://cds.cern.ch/record/2272264>.
- [22] Riccardo Del Burgo. The Tracker End-cap Pixel detector for CMS Phase-2 upgrade. Technical report, CERN, Geneva, Sep 2019. URL <https://cds.cern.ch/record/2706637>.
- [23] CMS Luminosity Based on Pixel Cluster Counting - Summer 2012 Update. Technical report, CERN, Geneva, 2012. URL <https://cds.cern.ch/record/1482193>.
- [24] CMS Collaboration. "CMS luminosity measurement for the 2018 data-taking period at $\sqrt{s} = 13$ TeV". Technical report, CERN, Geneva, 2019. URL <https://cds.cern.ch/record/2676164>.
- [25] S van der Meer. Calibration of the effective beam height in the ISR. Technical report, CERN, Geneva, 1968. URL <https://cds.cern.ch/record/296752>.
- [26] BRIL Ph2 Simulations Meeting. "Summary of Data Transfer Rates for Phase II Luminometers". . URL <https://indico.cern.ch/event/1011510/>.
- [27] G. Abbiendi et al. "The CMS muon barrel drift tubes system commissioning". *Nuclear Instruments and Methods in Physics Research Section A: Accelerators, Spectrometers, Detectors and Associated Equipment*, 598(1):192–195, 2009. ISSN 0168-9002. URL <https://doi.org/10.1016/j.nima.2008.08.100>. Instrumentation for Colliding Beam Physics.
- [28] Michail Bachtis. Upgrade of the CMS Barrel Muon Track Finder for HL-LHC featuring a Kalman Filter algorithm and an ATCA Host Processor with Ultrascale+ FPGAs. Technical report, CERN, Geneva, Oct 2018.
- [29] BRIL Ph2 Simulations Meeting. "Statistical precision and expected vdM statistical precision for Phase II luminometers". . URL <https://indico.cern.ch/event/1011510/>.